Damage Mechanisms and Energy Absorption in Composite Laminates Under Low Velocity Impact Loads

V. Lopresto and G. Caprino

Abstract An extensive study of the behaviour of composite laminates subjected to dynamic loads was carried out by the authors many years in order to understand the complex mechanisms of damage initiation and propagation under low velocity impact loads. A review of the main results is hereafter presented.

The problem is that many parameters are involved in an impact and the induced damage is very complex and not always visible. The present research efforts were undertaken to supply semi empirical and analytical models for the prediction of the impact response in terms of load curve, damage, involved energies and forces, independently of the particular laminate, its thickness and stacking sequence, matrix type and content, fibre type and architecture, fibre orientations and impact conditions such as tup and support diameter, load speed.

Experimental tests were carried out on different material systems varying the initial kinetic energy until the complete penetration. This allows the study of the start and propagation of the failure modes. From the load-deflection curves recorded, all the impact parameters involved like first failure and maximum load and energy, absorbed and penetration energy, were obtained. The influence of the thickness and stacking sequence so that the composite system, constrain condition and tup diameter on the impact parameters was evaluated. Destructive and non-destructive techniques were adopted to investigate the failure modes and the observed damage was correlated to the relative energies.

The analysis highlighted the importance of the penetration energy, U_p. An elastic solution available for circular isotropic plates loaded at the centre was modified to model the indentation and applied to the prediction of the load-displacement curve necessary to know the energy that cause the first failure. Interestingly, the force

V. Lopresto (✉) • G. Caprino
Department of Materials and Production Engineering, University of Naples Federico II,
P.le Tecchio 80, 80125 Naples, Italy
e-mail: lopresto@unina.it

S. Abrate et al. (eds.), *Dynamic Failure of Composite and Sandwich Structures*,
Solid Mechanics and Its Applications 192, DOI 10.1007/978-94-007-5329-7_6,

required for damage initiation under form of delamination was found to increase at the increasing of the thickness, t, following a power law whose exponent is very close to 1.5 of the contact law.

1 Introduction

Due to their brittleness and anisotropy, composite laminates are particularly sensitive to low velocity impact damage caused by accidental loadings imparted during fabrication or in service. This has lead to many studies concerning impact dynamics [1–4], mechanisms of failure initiation and propagation [4–8] and the correlation between impact energy, damage and residual material properties [4, 5, 9–12].

In some cases, parameters such as the maximum force achievable for an assigned energy level or the energy required to penetrate the body, are of major interest. The body panels of car, truck and rail vehicles must be designed in order to prevent penetration by foreign objects of known mass and velocity so that it becomes very useful to know the penetration energy. The absorbed energy is very important, for example, in Formula 1 race cars where it is necessary that the mechanical shock is not transferred to the human body. At the aim to ensure the driver's safety in high speed crashes, lightweight laminated composites are designed to absorb the race car's energy and limit the decelerations on the human body. In this field, in fact, the extreme racing speeds may lead to severe accidents with high amounts of energy involved.

In the design of metallic aeronautical structures, medium and high-velocity impact phenomena are of major concern, due to the danger of flying debris during the take-off and landing operations, and bird strike in cruising. For composite components, also low-velocity impact must be taken into account, because even a tool dropping on the structure during fabrication or maintenance activity can induce severe damage, resulting in a significant strength loss.

In aerospace structures, it is very important to correlate the internal damage that can occur during an impact such as delamination, fiber failure, matrix cracking to the residual properties of the structure. In particular, delamination is the most critical one since it causes significant loss in compression strength that represent the most severe load causing failure for buckling.

Delamination is a crack in the resin rich area between two adjacent layers. It was observed that delamination occurs after a threshold energy has been reached in presence of matrix crack [13]. Even if there is a common agreement on the mechanisms of initiation and growth of this failure during an impact event [8, 14, 15], a general approach for predicting this damage mechanism is absent. The complexity of the stresses in the vicinity of impacted point complicates the analysis. For example, Ref. [14] showed that delamination growth was governed by interlaminar longitudinal shear stress (σ_{13}) and transverse in-plane stress (σ_{22}) in the layer below the delaminated interface and by the interlaminar transverse shear stress (σ_{23}) in the layer above the interface.

A dangerous aspect is the difficulty to detect damage by visual inspection. A composite can severely damage without any external sign. The only external indication of an impact is the indentation, the plastic deformation due to the contact, left by the impactor on the laminate surface. It has brought to the concept of "Barely Visible Impact Damage" (BVID), usually adopted in the design of aeronautical structures: for adequate safety, a minimum laminate strength is required in the presence of a barely visible indentation. For an ease inspection operations, the ideal composite for aeronautical applications should exhibit an easily detectable visible indentation when a small internal damage area, resulting in a negligible strength loss, has been induced by an accidental impact.

It is important to find a relationship between external and internal damage at the aim to investigate about the residual properties without destroy the structure.

An extensive study of the behaviour of composite laminates subjected to dynamic loads was carried out by the authors many years in order to understand the complex mechanisms of damage initiation and propagation under low velocity impact loads. A review of the main results is here presented at the final aim to give useful information to predict the residual strength. In the first sections, the load-displacement curve recorded during each experimental tests carried out varying the initial kinetic energy, were studied at the aim to obtain information about the impact behaviour of the specimens: some characteristic points were individuated to correspond to the evolution of the inner damage. In correspondence of these points, the first failure and maximum load, the correspondent energies, the absorbed and penetration energy were calculated. After that, the influence of the thickness and stacking sequence, matrix type and content, fibre type and architecture, fibre orientations and impact conditions like tup and support diameter, load speed is investigated to find semi empirical and analytical models for the prediction of the impact response in terms of load curve, damage, involved energies and forces. The internal and external damage was investigated through destructive and non destructive testing.

Another topic again obscure at this time is the way through which the initial energy of the impactor is introduced into the target. In a non-perforating impact, a part of this energy is stored elastically, and can be easily measured. Particular attention is dedicated, in Sect. 3.4, to the elastic energy that causes the first failure, generally found as delamination. At the aim to predict this critical value, it is necessary to accurately describe the load curve and to know the critical force resulting in the first failure. At this scope, a non-linear solution available for isotropic materials [16] was modified and it was revealed valid to accurately shape the elastic portion of the load curve and to predict the contact force corresponding to delamination initiation and the related energy. The results show a very reasonable agreement with the theory.

An indentation law, allowing for the prediction of the impact energy from the depth of indentation, was assessed and presented in Sect. 3.6. This law has a general applicability, being scarcely affected by the fibre type and orientations, and matrix type. The indentation was found to be a function of the impact energy through the perforation one that represent the kinetics initial energy necessary to

completely penetrate the laminate and obtained as the area under the complete load curve at penetration [17]. The latter becomes a fundamental parameter to be known at the aim to have information about the impact energy that cause the strength loss [9, 18–20]. The complex failure mechanisms that can occur in a laminate under low velocity impact load and their complex interaction must be taken into account too. The impact tests revealed that, for a given fibre areal weight, U_p was independent of the reinforcement architecture and stacking sequence and of the extend of the delamination. U_p increases more than linearly with thickness times fibre volume fraction, confirmed in [21–23]: the dependence found for CFRP and GFRP laminates is well described by a power law having exponent 1.5 and 1.35 respectively. This is discussed in Sect. 3.7.

The dependence of the residual strength on the impact energy and the possibility to predict the residual properties of the composite structures from indentation depth measurements by a minimum of experimental tests is included in the successive section.

Efforts were done, and the results are presented in Sect. 3.9, at the aim to establish a correlation between the damage occurring in a composite as a consequence of low-velocity impact and the energy dissipated during the impact phenomenon. To investigate about the damage progression as a function of impact energy, ply-by-ply delamination and fibre breakages revealed by destructive tests were measured. A previous model, based on energy balance considerations, was applied to understand the experimental results, together with an original method of data reduction, allowing for the isolation of the maximum energy portion due to indentation and vibrational effects.

The damages were observed by visual analysis, as well as by deplying some of the specimens: delamination was found between layers equally oriented too.

2 Materials and Experimental Methods

During the history of the present experimental research, a large variety of samples (Table 1) were tested under very different tests conditions. Most of them concerned carbon fibre laminates made of prepreg with fibres T400/HMF 934 epoxy resin under form of tape and fabric with different fibre areal weights, stacking sequences and thicknesses. The thickness varied in the 1–4 mm range that is generally considered for applications. Quasi-isotropic panels with $\{[(0, 90)/(\pm 45)]_s\}_n$ stacking sequence, $n = 1$ to 4, were fabricated by hand lay-up and autoclave cured at 177 °C under 0.7 MPa pressure. The fibres were under form of plain weave fabric 193 g/m^2 in areal weight. The specimens were labelled as F in the text. The stacking sequence $[(0, 90)_n/+45_n/-45_n]_s$ was adopted too for the same presented material and technology (FT label). The fibre content by volume was $V_f = 0.55$. Moreover, rectangular graphite/epoxy panels, labelled as T30, T60 and T45, made of carbon/epoxy T400/934 tape were fabricated with different lay-ups, $(\pm 30)_{2s}$,

Table 1 Materials tested in the present work

ID	Material	Lay up	t (mm)	V_f (%)	D_t (mm)	D_s (mm)
F	T400/HMF 934	$\{[(0, 90)/(\pm 45)]_s\}_n$ n = 1 to 4	0.96–3.85 (1–4)	55	12.7, 16, 19.8	40, 50
FT	T400/HMF 934	$[(0, 90)_n/+45_n/-45_n]_s$	0.95–3.80 (1–4)	55	6–19.8	50, 100
T30	T400/HMF 934	$(\pm 30)_{2s}$	1.2	55	6–19.8	50
T60	T400/HMF 934	$(\pm 60)_{2s}$	1.2	55	6–19.8	50
T45	T400/HMF 934	$(\pm 45)_{2s}$	1.2	55	6–19.8	50
SMC	–	–	1.7–7	30	6–20	40–100
(C50/50)	E-glass/epoxy	$(0/90)_n$ n = 5–16	0.7–2.4	60	6–20	50–100
(C90/10)	E-glass/polyester	$(0/90)_n$ n = 4–8	1.2–4.2	35	6–20	50–100
G	E-glass fabric 295 g/m^2 in areal weight and Cycom 7701 epoxy resin	$[(0,90)_n/(+45,-45)_n]_s$ n = 1 to 4	0.96–3.85	55	16, 19.8	50

$(\pm 60)_{2s}$, and $(\pm 45)_{2s}$, resulting in laminate nominal thickness t = 1.2 mm. The fibre content in the cured laminates was about 55% by volume, and the total fibre areal weight 1.16 Kg/m^2. Three basic laminae, namely a sheet moulding compound and labelled as "SMC" hereafter, an E-glass cloth/epoxy with 50% fibre in the warp and 50% fibre in the weft direction (C50/50), and an E-glass cloth/polyester with 90% fibre in the warp and 10% fibre in the weft direction (C90/10), were used to obtain additional composite plates tested in the present campaign. The fibre volume fraction V_f was 0.30, 0.60, and 0.35, respectively, and the nominal thickness of a single cured layer 0.6, 0.15, and 0.3 mm. For each material system, panels different in thickness were fabricated stacking together different numbers of layers. In the C50/50 and C90/10, the layers were laid to obtain 0/90 balanced laminates having a total of 50% fibre along the 0° and the 90° directions. The panels were cured under press according to the resin supplier specifications, and from them square specimens, 150 mm in side, were cut by a diamond saw.

Also GFRP prepreg made of plain-weave E-glass fabric 295 g/m^2 in areal weight and Cycom 7701 epoxy resin were used to fabricate square plates 300 × 300 mm cured by a stamp forming process between hot press plates at 120 °C of temperature and 2 bar of pressure for about 2 h. The stacking sequence was $[(0,90)_n/(+45, -45)_n]_s$, with n = 1 to 4, and the corresponding nominal thicknesses *t* varied in the range 0.96 mm to 3.85 mm. The fibre volume fraction was about 55%. The specimens cut are labelled as G in the text.

From the panels, square and rectangular specimens were cut by a diamond saw and subjected to the experimental tests. They were supported on steel plates with a circular opening 40, 50 or 100 mm in internal diameter, D_s in the last

column of Table 1, or on a rectangular window 150×100 mm suggested by the EN6038, respectively. All the low-velocity impact tests were carried out on a Ceast Fractovis MK4 instrumented falling weight testing machine, equipped with a DAS 8000 digital acquisition system. Specimens were struck at their centre using hemispherical steel indentors with diameters $D_t = 12.7$, 14.9, 16 or 19.8 mm. To prevent multiple impacts, the tup was caught on the rebound by a brake available in the test apparatus.

A first series of tests, to obtain and record the force-displacement (F-d) curve at perforation, was carried out using a mass $M = 10.6$ kg falling from a 1 m height. From the F-d curves recorded for each panel, the penetration energy was evaluated. The different energy levels were produced by suitably combining the drop height and three masses ($M = 3.6$, 5.6, 7.6 kg) available in the testing machine. In all, at least five impact tests were performed for each experimental condition.

Additional tests carried out on a MTS RT/50 universal testing machine in displacement control statically loading the specimens, had the scope to investigate about the influence of the loading speed and the possibility to study the impact phenomenon by static conditions. The adopted supports and impactors were the same of the dynamic tests. The stroke speed was fixed at 0.1 mm/min.

All the involved energies were evaluated by numerical integrations as the area under the load-displacement curves recorded. The force values were evaluated directly on the load curve. The indentation resulting from the indentor-material contact was measured by a micrometric dial gauge and the measurements were performed following the EN6038 standard.

After impact, each specimen was visually inspected to ascertain eventual visible damage. The coupons were, then, inspected by an ultrasonic (UT) pulse-echo immersion testing technique and, after a transversal cut suggested by the NDE results, analysed by an optical microscope, Leitz, in order to identify damage modes.

Some of the E-glass specimens struck with $D_t = 19.8$ mm were subjected to a deeply technique too. First of all, after impact, since glass fibres are transparent, the extent of the projected delaminated area was obtained exploiting the translucent appearance of the material: the damage zone was highlighted by an intense light source on the back of the specimens, and photographed; then, the projected damage area was measured by an image analyzer and related to the specimen thickness and the impact energy. In order to study the ply-by-ply damage extent and type, a small hole 1 mm in diameter was drilled in correspondence of the impact point of the selected specimens. The aim was to ease the penetration of the liquid into the interlaminar cracks. The specimens were immersed in blue ink bath for 1 h until the projected delaminated area was completely darkened by the ink; then, they were dried for a suitable time of about 2 h, and carefully thermally deplied with the help of moderate heating; finally, the resin was burnt away and the delaminated area in correspondence of each interlaminar surface was measured, and the in-plane length of broken fibres within each ply was evaluated by optical microscopy at low magnification.

3 Experimental Observations

3.1 Load-Displacement Curve

The load-displacement curve recorded during a low velocity impact at complete penetration contains useful information about the failure process: it is possible to observe, characteristic points related to the behaviour of the material under dynamic loads. Despite differences in thickness, material and architecture, these curves showed some features common to all laminates [24, 25]. Figure 1 shows a schematic view of a typical load-displacement curve with several characteristic points. In Fig. 2, four different curves recorded during low velocity impact tests on

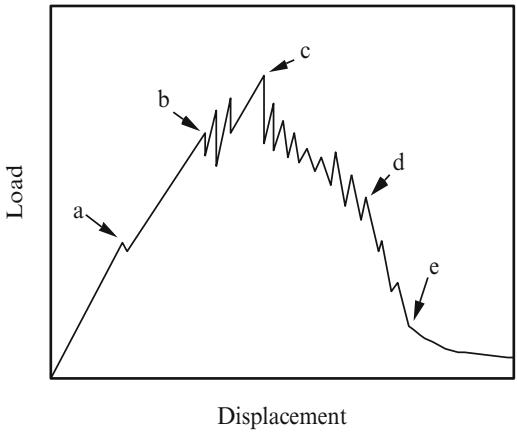

Fig. 1 Schematic view of the impact load displacement curve at penetration

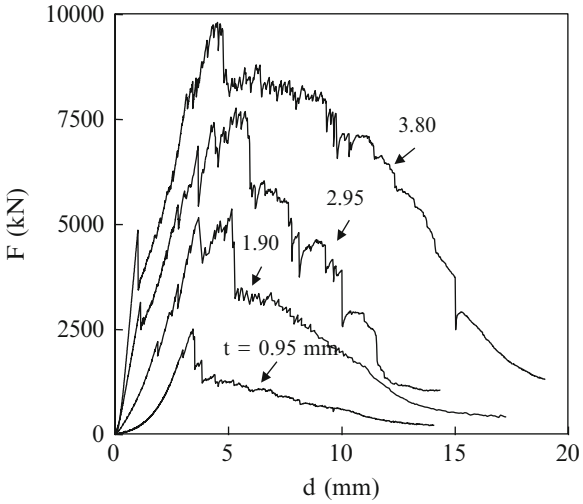

Fig. 2 Load curves for different thickness: mat. FT from Table 1; $D_s = 19.8$ mm

CFRP laminates (FT from Table 1), one for each different thickness, are collected. Despite the difference in thickness, some common features were noted.

Up to point "a" in Fig. 1, the curve shows no evidence of damage developing inside the material. In this diagram a linear trend is observed initially as the displacement increases.

However, a different behaviour between thin (less than eight layers) and thick laminates was observed as showed in Fig. 2 where the initial rigidity of the laminates increases with increasing t. The thinnest plates display an evident non-linear response under very low displacement values (less than 2 mm in Fig. 2), due to large displacements [26].

At the end of the elastic phase a load drop, clearly visible when the material thickness is sufficiently high, is noted (point "a" in Fig. 1). This is difficult to appreciate for the lowest thickness where the load remained substantially constant with increasing the displacement or a different slope is evidenced, with only negligible oscillations. However, in both thin or thick laminates, a local rigidity variation happens, denoting damage inside the laminate.

The successive drop of the load is an indication of damage initiation in the form of fibre breakage, and/or damage propagation in the form of matrix cracking and delamination, fibre breakage, and fibre/matrix debonding and pull out (point b on the curve). Matrix cracks in the resin pockets, are commonly believed to be the first type of damage during an impact [26, 27] and the presence of matrix cracks does not dramatically affect the overall laminate stiffness during an impact event [25, 28]. However, matrix cracks represent the initiation point for delamination [14, 18, 29, 30] and fibre break that dramatically change the local and the global stiffness of the composites and influence the load–time response [31]. All the energy that exceed the latter is used for the propagation of the damages. Of course, all these failure modes lead to a reduction in the residual strength of the impacted panels [25]. After first failure, the load increases again, although the laminate rigidity is reduced. Then, a series of load drops, resulting in oscillations in the force-displacement curves, are noted to correspond to extensive failures in the fibres and in the resin along the laminate thickness.

In the range "b" – "d", the different damage propagate through all the layers that are progressively broken, until (point "d") the complete perforation. The term "perforation" is used here to indicate that there is at least one fracture surface in each layer, so a light beam can pass through the laminate. The slope of the F-d curve begins to decrease rapidly when the material perforation occurs.

The maximum force (point "c" in Fig. 1) was generally achieved between points "b" and "d" even if for the thickest laminates (twelve layers or more), the point b was often found coincident to point d that means that the first significant fibre failure often happens at maximum force [24].

The decrease in the contact load between "d" and "e" is about the penetration process. Finally, beyond point "e" the contact force decreases slowly: the cylindrical impactor slides along the penetrated sample and the energy is dissipated by friction. The penetration energy, the difference between the initial and residual kinetic energy

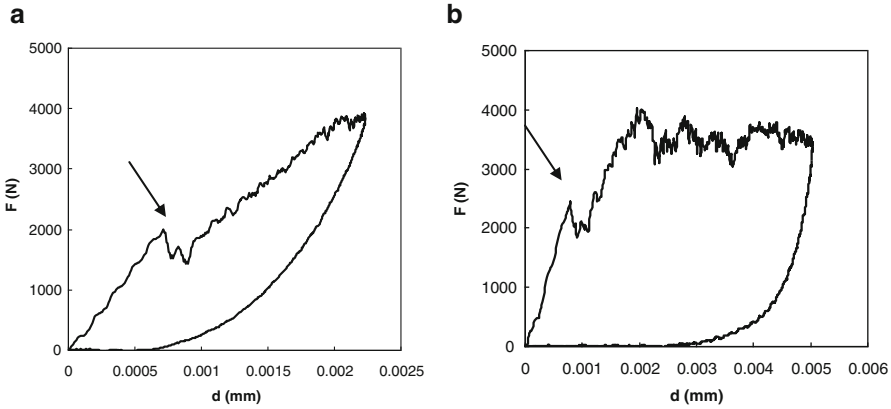

Fig. 3 Load-displacement curve of a 3 mm non penetrated carbon fibre laminate. (**a**) impact energy level U = 5 J; (**b**) impact energy level U = 15 J

of the projectile, necessary to completely penetrate the laminate and given by the area under the load-displacement curve at penetration, is conventionally calculated at point "e".

Both Figs. 1 and 2 deal with cases in which complete perforation occurs. In case of non-perforating impacts, at some point the projectile reaches a maximum displacement and then the displacement decreases during unloading (Fig. 3). After the first load drop (arrows in Fig. 3), the unloading part is different from the loading one since a part of the energy is stored inside the material for the damage formation. In Fig. 3, in fact, where the curve refers to a specimen loaded by 15 J of impact energy, it is possible to note a larger area respect to Fig. 3 where the same laminate was impacted by a lower energy, U = 5 J, that caused less damage. The first load drop signalled by the arrow in Fig. 3 is generally due to delamination that was found the only damage when the 3 mm specimen was impacted with 5 J of energy. A higher impact energy of 15 J caused the propagation of the damage along the thickness in correspondence of a nearly constant load.

Since the similar shape of the curves in Fig. 2, a scaling coefficient was adopted to overlap the curves: by scaling the force according to the coefficient 1.5, the same force-displacement curves sensibly converge to a single master curve, the displacements are held unchanged (Fig. 4). Therefore, the contact force varies according to $t^{1.5}$. All the curves were normalised for the thickness 3.06 mm (16 layers laminate). In this way, as it will be hereafter discussed, the dependence of the first failure load, maximum force, energy at maximum force and penetration energy on the thickness can be easily established. By using a scale parameter in the design of experiments for impact damage the number of experimental tests can be reduced.

Other investigators [21] have also used a scaling parameter, able to predict the force-displacement curve exhibited by thick laminates, obtained using the force-displacement curve recorded in testing thin samples. From the experimental data,

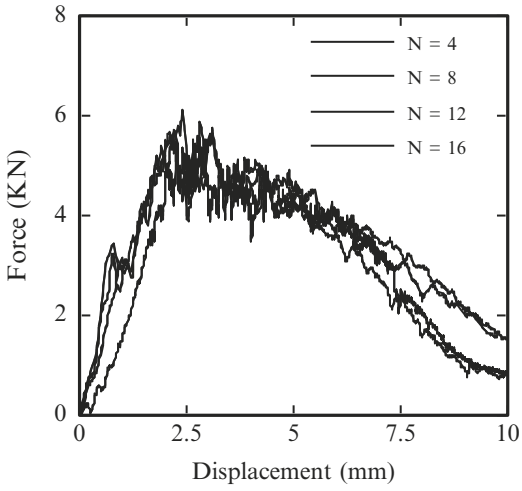

Fig. 4 Superposition of the force-displacement curves for the different thicknesses. *N* number of layers

concerning composite plates having thicknesses in the range 3.3–8.3 mm, all the curves were reduced to a master curve, by scaling both the force and the displacement through power laws. The best scaling exponent for forces was 1.2, whereas the best exponent for the displacements was 0.35. Considering that energy is the area under the force-displacement curve, it was concluded [21] that the penetration energy varies to the power of 1.55 with increasing the plate thickness. It is very similar to the exponent 1.5 found in this work.

Carefully observing the curves in Fig. 4, the superposition does not hold in the very early stage of contact because, as it will be demonstrated, the energy in correspondence of delamination initiation does not increase according to a power law. After perforation, the superposition is satisfying for the 4 and 8 layers laminates and for the 12 and 16 layers composites denoting a drastic change in the failure modes after perforation for the two different groups of thickness.

3.2 Force at Damage Initiation

In this section the effect of several parameters on the damage initiation force is studied. Those parameters are: the laminate thickness, the diameter of the impactor, and the size of the plate. The trends observed are compared with prediction from simple models.

Laminate thickness strongly affect the contact force history. The influence of material thickness on the force at damage initiation, F_i, was first evaluated. The importance in predicting the first failure load is due to the fact that it represents a threshold for the formation of a damage that is not always possible to individuate on the load curve. This force was here evaluated in correspondence of the first load drop

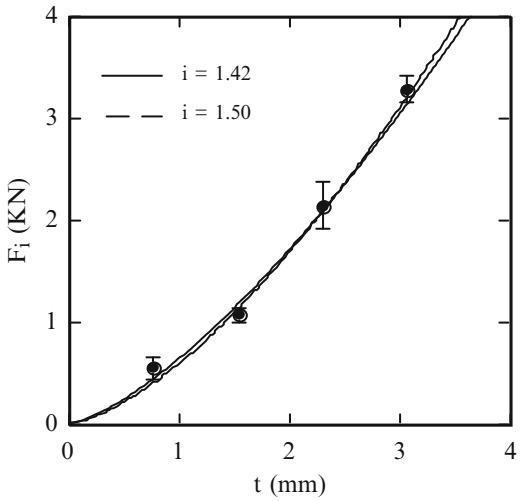

Fig. 5 Force for damage initiation, F_i, against specimen thickness, t

or the change in slope on the ascending portion of the load *vs* displacement curve (point "a" in Fig. 1). The data were obtained loading CFRP specimens made of T400 fibres and HMF 934 epoxy resin having $\{[(0, 90)/(\pm 45)]_s\}_n$ stacking sequence, with $n = 1$ to 4, resulting in nominal thicknesses varying in the range 1–4 mm (F in Table 1). It was found that F_i follows a power law as a function of the thickness, with the exponent coincident with the exponent of the contact law.

Studying the contact between a rigid sphere and a laminate some researchers [32–35] demonstrated the successful application of the elastic contact law [36]. In Fig. 5, F_i is plotted against the specimen thickness, t, for the data obtained here.

The following expression:

$$F_i = F_{io} \cdot t^i \tag{1}$$

was revealed adequate to describe the F_i trend (continuous line in Fig. 5). From the best-fit curve, the values $F_{io} = 0.64$ KN/mm^i and $i = 1.42$ were obtained, for F_i given in KN.

According to the Hertzian contact law [36], the radius R of the contact zone is given by:

$$R = k \cdot \sqrt[3]{D_t \cdot F} \tag{2}$$

where k is a constant only depending on the material elastic constant [36], F is the applied load and D_t the impactor diameter.

For a circular plate loaded at the centre, the shear stresses in the thickness direction around the point of load application are dependent on the applied load, rather than on the flexural moment. In fact, the evaluation of the shear force per unit length of arc along a circle of given radius only involves equilibrium considerations.

A shear induced failure develops when the average shear stress τ along the thickness direction at the periphery of the contact zone achieves a critical value, proportional to the interlaminar shear strength $\bar{\tau}$ of the material:

$$\tau = k' \cdot \bar{\tau} \tag{3}$$

where k′ is a constant.

From equilibrium considerations, considering the cylindrical shape along the thickness in correspondence of the contact zone, it results that the average shear stress τ along the specimen thickness at the boundary of the contact zone is:

$$\tau = \frac{F}{2\pi R t} \tag{4}$$

where t is the laminate thickness. It is necessary to underline that this is an approximate formula since τ is not the maximum value but the mean value along the thickness.

If the shear stress is responsible for delamination initiation, from Eq. (2) and (4) F_i was calculated as:

$$F_i \propto (\bar{\tau} \cdot t)^{1.5} \tag{5}$$

where $\bar{\tau}$ is the interlaminar shear strength of the material.

A good agreement between the exponent of Eqs. (1) and (5), related to the experimental value (i = 1.42) and the expected one from the contact law, was respectively found. It is possible to better appreciate the agreement between experiments and theory in Fig. 5 where the dashed line was drawn putting i = 1.5 in Eq. (1), and F_{io} =0.60 KN/mm$^{1.5}$ by the best fit method. In this way, a simple failure criterion uniquely based on shear stresses would be able to calculate the critical load for delamination initiation.

Matrix cracks are believed to be the first type of damage during impact. It has been shown by Sjoblom et al. [28] that the presence of matrix cracks does not dramatically affect the overall laminate stiffness during an impact. It was demonstrated that [30, 37, 38] an interaction between matrix cracking and delamination initiation exists. Matrix crack tips act as starting points for delaminations and fibre breaks and the latter two damages can dramatically change the local and or global stiffness of the composite laminate and effect the load-time response [31]. Delamination propagate starting from intralaminar cracks was found in particular in thin laminates [38–41] where the membrane contribution is significant. In the following figures, low (a) and high (b) magnification micrograph of loaded quasi-static (Fig. 6) and dynamic (Fig. 7) beam showing the matrix and delamination cracks resulting from quasi-static bending are reported [38]. The same was confirmed here by the authors: for example, in Figs. 8 and 9 a central part and a magnification of the central thickness of a micrograph showing delamination starting from cracks in the resin pocket and connected by intralaminar cracks in the FT laminate 2 mm in thickness (Table 1), is reported.

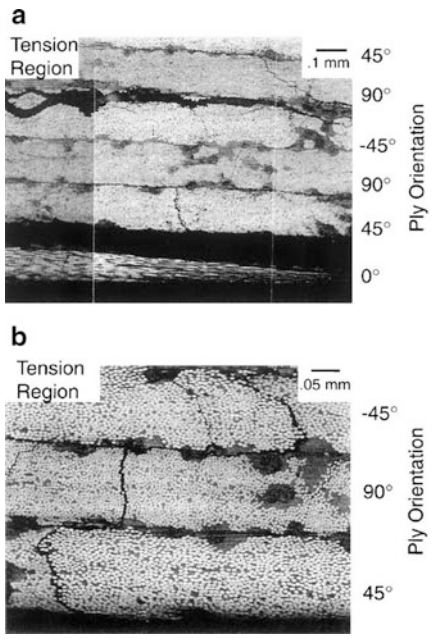

Fig. 6 Low (**a**) and high (**b**) magnification micrograph of the tested quasi-static beam showing the matrix and delamination cracks from quasi-static bending

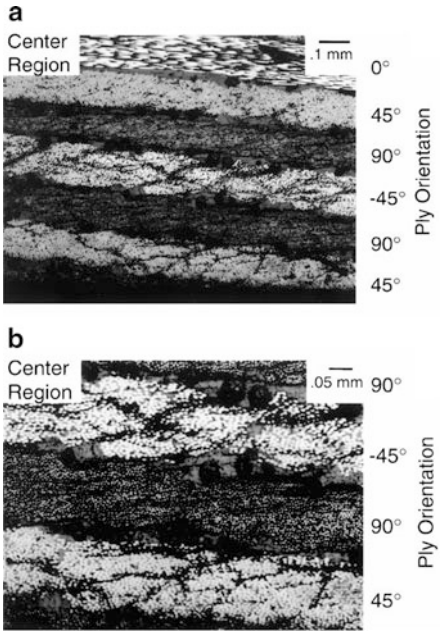

Fig. 7 Low (**a**) and high (**b**) magnification micrograph of the dynamically tested beam showing matrix and delamination cracks. V = 34.9 m/s

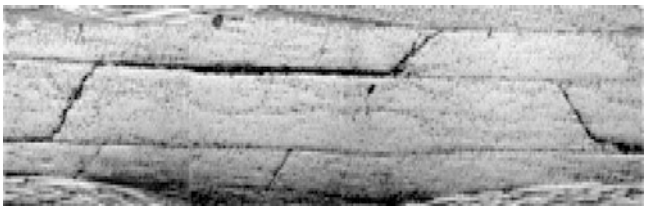

Fig. 8 Micrograph showing delamination starting from cracks in resin pocket and connected by intralaminar cracks in FT laminates (Table 1), t = 2 mm

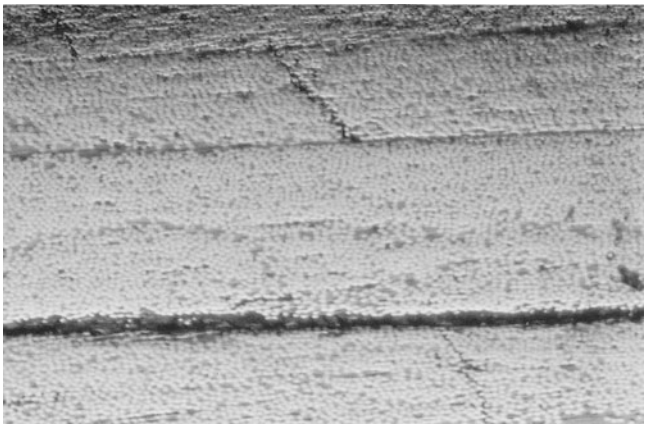

Fig. 9 Magnification of the central part of a micrograph showing delamination starting from cracks in resin pocket and connected by intralaminar cracks in FT laminates (Table 1), t = 2 mm

As accepted by a large number of authors [14, 30, 42, 43], the evolution of the damage in a composite laminate subjected to a concentrated force is driven by intralaminar tensile and shear cracks occurring in the layers farther from and nearer to the contact point. From these cracks, delaminations were found to be generated at interfaces between plies with different orientations, mainly propagating in the direction of the fibres in the lower ply, and extending the more, the larger is their distance from the contact point. These mechanisms were, here, observed only in the thinnest laminates. By deplying GFRP laminates, for $t > 0.96$ mm, delamination was found between layers with the same orientation too, in agreement with [44, 45]. In particular, for $t = 2.88$ mm the maximum extent of interlaminar fractures was found at the midplane between layers having the same orientation.

Extensive delamination was also found without macroscopic evidence of intralaminar cracks in the thick laminates. This confirms that in thick plates shear stresses play a main role for delamination initiation [39–42, 46]. In [39–41, 46], the problem of the delamination initiation was investigated in depth. A difference between thin and thick laminates was found. In the thin laminates the bending

is predominant whereas the shear stresses predominates in the thick ones and delaminations without intralaminar cracks evidence were found at the mid plane.

Sjoblom [47] proposed a simple model for the calculation of F_i based on the hypothesis that the first failure happens when the shear stress τ along the direction of the thickness attains a characteristic critical value τ_c. Taking into account also the effect of the tup diameter, D_t, from the contact law, [47], F_i was calculated as follow:

$$F_i = \frac{(2\pi\tau_c)^{1.5} D_t^{0.75}}{k_c^{0.5}} \tag{6}$$

where k_c is the local rigidity. From Fig. 2 the first load drop becomes lower and lower at the decreasing of laminate thickness since most of energy is stored to the bending phase.

Combining Eqs. (2), (3) and (4), F_i is easily obtained as [48]:

$$F_i = \delta D_t^{0.5} t^{1.5} \tag{7}$$

where:

$$\delta = \left(2\pi \cdot k \cdot k' \cdot \overline{\tau}\right)^{1.5} \tag{8}$$

dependent on τ_c and k_c.

Equation (7) is coincident with Eq. (5), except for the fact that in the latter the influence of the tup diameter is not explicit.

Of course, Eq. (7) is expected to lose its validity when the first failure takes place in the back layer of the laminate. In this case, since the flexural moment depends on the support diameter, the phenomenon should be strongly affected by this parameter.

In Fig. 10 the term $F_i/D_t^{0.5}$ is plotted against the thickness, t: all the data about the FT laminates converge to a single curve irrespective of the tup diameter and the velocity (some data are, in fact, from static tests). Only in the case of small thickness of $t = 0.95$ mm loaded by a large indenter diameter, $D_t = 19.8$ mm, the superposition is not verified (circle in Fig. 10). In this case the flexural rigidity is low (low thickness) whereas the first failure load is relatively high since the large tup diameter. The curvature at first failure is so large and this impairs the model on which Eq. (7) relies.

The continuous line is drawn by Eq. (7). The constant value of 0.152 KN/mm^2 was calculated best fitting all the experimental data except the one, the triangle symbol in the circle in Fig. 10, that does not follow the general trend.

For the thinnest laminate supported on the fixture 50 mm in diameter and loaded with the 12.7 mm tup diameter it was not clearly apparent from the curve the first load drop, so that only the non-destructive analysis was able to approximately detect the first failure point. The same difficulty was not found when the 19.8 mm tup diameter was adopted, without varying the support diameter (arrow in Fig. 11).

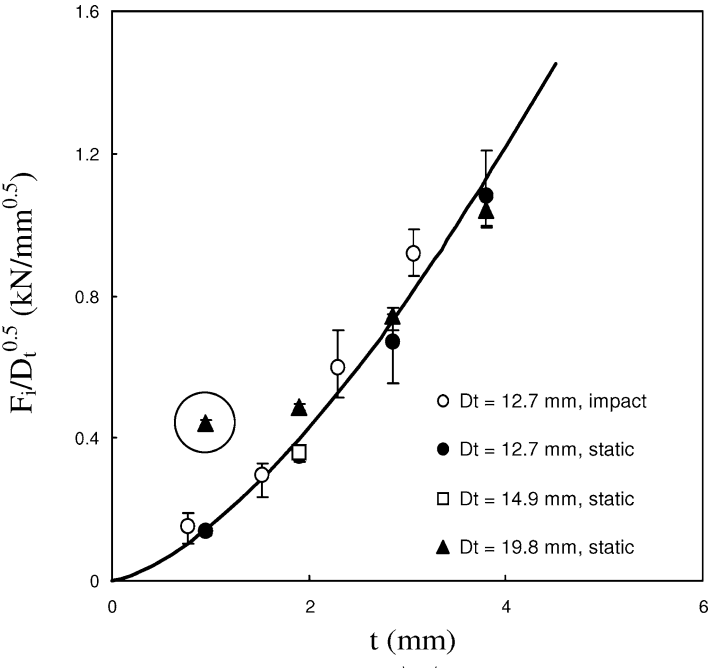

Fig. 10 Effect of the laminate thickness, t, and tup diameter, D_t, on the first failure load, F_i. Mat.: FT (Table 1)

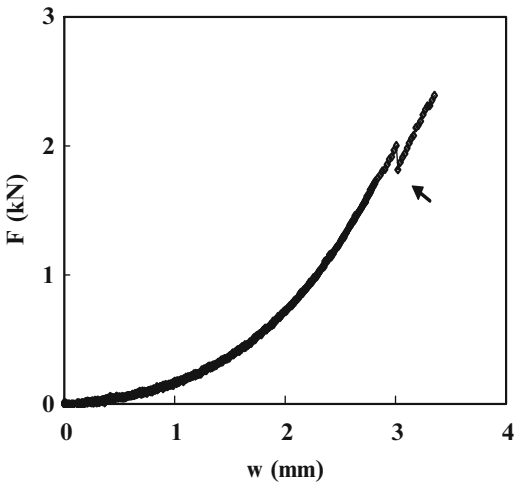

Fig. 11 Load-deflection curve at first failure t = 0.95 mm and a tup diameter D_t = 19.8 mm. Support diameter D = 50 mm

One of the hypotheses on which Eq. (7) relies is that the first failure is independent on the support diameter, being uniquely determined by the shear stresses, rather than by the normal stresses associated with the flexural moment.

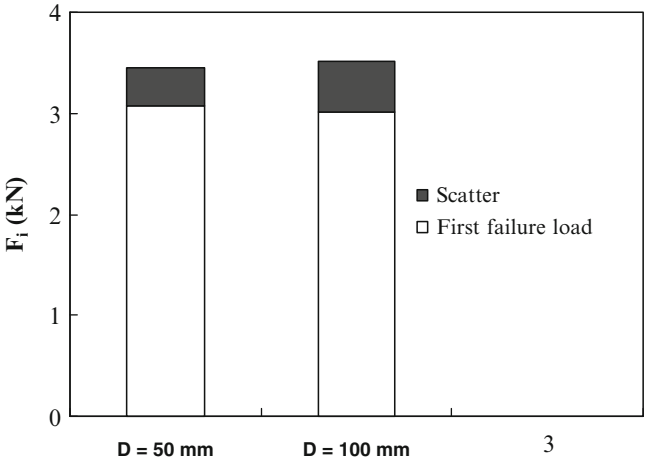

Fig. 12 Effect of the support diameter, D_s, on the first failure load, F_i. Plate thickness t = 2.85 mm; tup diameter D_t = 19.8 mm. Mat.: FT laminates (Table 1)

Fig. 13 First failure load, F_i, vs plate thickness, t, for a tup diameter D_t = 19.8 mm. Support diameter D_s = 50 mm

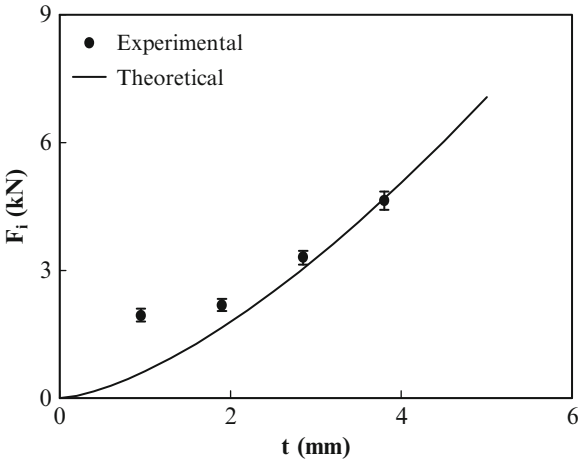

In Fig. 12, the first failure loads recorded in the tests carried out by adopting D_s = 50 mm and D_s = 100 mm for t = 2.85 mm and D_t = 19.8 mm are compared. The load inducing first failure is actually the same, independently of the support diameter which confirms the assumption made.

Comparing Eqs. (1) and (7) and accounting for the tup diameter (D_t = 12.7 mm), the δ value of 0.142 kN/mm^2 is immediately calculated from F_{io} = 0.507 kN/mm$^{1.5}$. Then, from Eq. (7) the critical load F_i was calculated as a function of t with D_t = 19.8 mm (continuous line in Fig. 13).

From the comparison of theory with the experimental data, the agreement is quite good for thick laminates whereas for thinner plates the predicted trend diverges from the actual one. An explanation of this occurrence is given hereafter.

Eq. (2), from which the first failure criterion is derived, is rigorously valid for a sphere impinging a flat plate. When the real plate is loaded with an increasing force, its curvature increases accordingly, so that Eq. (7) falls in defect. In particular, the actual contact area becomes larger than predicted from Eq. (7) [36]. As a consequence, the average shear stress (Eq. 4) decreases and the critical load F_i increases. This effect is more evident for thin than for thick plates, since their higher deflection for a given applied force. This explain why F_i is higher than expected for the thin laminates in Fig. 13. On the other hand, from the theory of Hertzian contact, the error in using Eq. (7) rapidly increases with increasing D_t. Therefore, the validity of this equation is anticipated to hold within a higher range of plate thicknesses for lower tup diameter values. This can justify the agreement between theory and experiments in Fig. 13.

From Eq. (7), the first failure load for the plates with $t = 1.9$ mm loaded by a 14.9 mm tup diameter was calculated, obtaining $F_i = 1.44$ kN. From three tests carried out on $D_s = 50$ mm, the mean value $F_i = 1.38$ kN, in good agreement with the theoretical prediction, was obtained. This result seems to confirm that the usefulness of Eq. (7) is retained if the tup diameter is small enough. When the scope of the test is the material characterisation in terms of δ, small tup and support diameters, and high plate thicknesses should be used to avoid large deflections of the plate, favouring the applicability of Eq. (7).

The simple dependence of the first failure on the specimen thickness independently of the tup diameter is in a complete agreement with the results published in [27] where about 350 specimens different in thickness and laminations and made of three different types of basic laminae were examined at the aim to investigate about the first failure load. The first failure load was found to vary with the laminate thickness to the 3/2 power too. The same was predicted by other investigators [47, 49–52]. Moreover, in [42] where the impactor diameter and the boundary conditions were fixed, F_i was found to be dependent on $t^{1.5}$ and the critical shear strength was found to be a constant value for the specific material system even if the laminates are made of laminae with different orientations.

3.3 Energy at Damage Initiation

Since the energy, rather than force, is the input datum in impact, one of the most important objectives in approaching the problem of impact is the possibility to predict the energy level in correspondence of which the first damage begins to develop. In what follow, the main factors affecting the absorbed energy at damage initiation are examined and from the results an analytical model is developed. The model allows the calculation of the first failure energy assuming that the total energy is shared in two parts, one of which stored in flexure, and the other in the material volume close to the contact zone.

The main energy absorbing mechanisms can be partitioned into, U_{flex}, the energy stored by the plate in bending; U_{ind}, is absorbed due to the localised contact deformation; some energy is dissipated through vibrations. It is difficult to separate the irreversibly absorbed energy that contributes to damage initiation and propagation. Many authors [53–56] have shown that, for sufficiently low velocity impact, that means up to 10 m/s [10, 28, 52, 57], the behaviour of carbon fibre reinforced plastics is independent of the loading rate, so that the dynamic response can be simulated by static tests. The energy dissipated by vibrations is negligible, and the flexural displacement w_o can be modelled by strength-of materials formulae. The same does not happen for GFRP laminates [58, 59] since the viscoelastic nature of the glass fibres.

Therefore, it can be assumed that, in a low velocity impact, the penetration of CFRPs energy is the sum of two components: one related to the flexure of the panel, and the other related to failure modes. A composite plate subjected to a transverse load absorbs energy by deformation and creation of damage zone. The material deformation occurs first and the panel absorbs energy through flexural deformation. This part of energy has been identified by elastic energy, U_{flex}. It is expected that the capacity to store elastic energy increases as the panel dimensions increase, since the flexural deformation will be larger, or when it is less constrained at the supports. In addition, plate deflections are proportional to the bending rigidities which in turn are proportional to the cube of the plate thickness [60] so that the decrease of the thickness has the same effect of the increase the panel dimension. In these cases, the structural rigidity became lower, provided the failure modes remain unchanged. U_i represents the limit energy below which no damage is present in the laminate. Energies supplied higher than U_i, are useful for damage initiation and propagation at perforation.

With these hypotheses, the energy absorbed by the material at the point of delamination initiation is given by:

$$U_i = \int_0^{w_t^*} F dw_t \tag{9}$$

where F is the applied load, $w_t = w_o + w_i$ where w_i is the indentation, w^*_t is the critical deflection at first failure, and

$$w_0 = K_f \frac{F}{D} \tag{10}$$

with K_f a constant depending on the boundary conditions and D the flexural rigidity, which for an orthotropic circular clamped plate can be calculated as the elements D_{ij} of the [D] matrix, through the relationship available in [16].

For the contact law, the following relationship holds:

$$F = K_{ind} \cdot w_i^{1.5} \tag{11}$$

Substituting w_o and w_i from Eqs. (10), (11) in Eq. (9) and integrating, it was possible to obtain U_i as:

$$U_i = \frac{K_f F_i^2}{2D} + \frac{2F_i^{5/3}}{5K_{ind}^{2/3}} \tag{12}$$

where the first and the second term on the right represent U_{flex} and U_{ind}, respectively.

From Eqs. (12) and (1):

$$U_i = \frac{K_f \cdot F_{io}^2 \cdot t^{2i}}{2D} + \frac{2F_{io}^{5/3} \cdot t^{5i/3}}{5K_{ind}^{2/3}} \tag{13}$$

From lamination theory, it can be verified that, for all the laminates taken into account:

$$D = K_D \cdot t^3 \tag{14}$$

with K_D a constant.

Since the dependence of F_i on the laminate thickness can be predicted very well by a power law having exponent $i = 1.5$ (see dashed line in Fig. 5), in the following this value will be adopted for simplicity. In fact, this assumption is in agreement with the hypothesis of contact law, underlying Eq. (13) (see Eq. (11)). Accounting for this and combining Eq. (13) and Eq. (14), it is finally found:

$$U_i = \frac{K_f \cdot F_{io}^2}{2K_D} + \frac{2F_{io}^{5/3} \cdot t^{2.5}}{5K_{ind}^{2/3}} \tag{15}$$

Therefore, according to Eq. (15), U_{flex} should be independent of the thickness, t, whereas U_{ind} should vary with $t^{2.5}$.

In Fig. 14, the measured U_i is plotted against t. It was found to increase rapidly with increasing the thickness of the laminate.

Plotting the data in Fig. 14 against $t^{2.5}$ as predicted from Eq. (15), the experimental points fall with excellent agreement along a solid straight line having equation:

$$U_i = 0.318 + 0.047t^{2.5} \tag{16}$$

with U_i in J and t in mm. From this equation, the U_{flex} is 0.318 J (dashed line in Fig. 14). This energy could be calculated from the first term on the right of Eq. (12), knowing that, for a clamped plate loaded by a concentrated force at the centre, the constant K_f is given by [16]:

$$K_f = \frac{R^2}{2\pi} \tag{17}$$

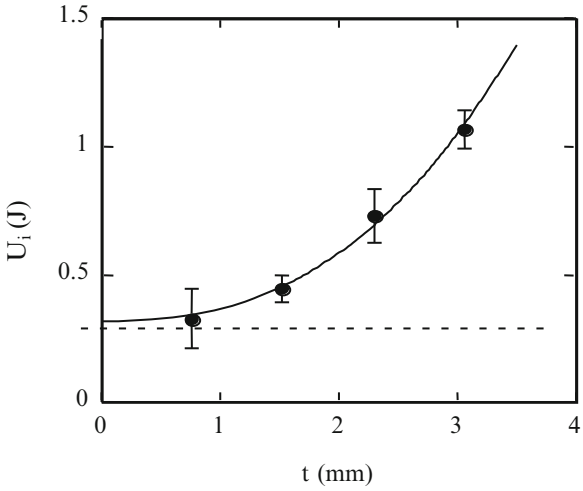

Fig. 14 Energy for damage initiation, U_i, against specimen thickness, t. Mat.: F (Table 1)

where R is the plate radius.

In [32], a different value of the constant affecting the second term on the right of Eq. (16) (0.016 KN/mm$^{1.5}$) is calculated from Eq. (15). The poor agreement with the experimental value found here (0.047 KN/mm$^{1.5}$) is due to fact that the resin type or the fibre form (fabric in the present case, unidirectional in [32]) play a major role in lowering the local rigidity of the material. Consequently, the relative importance of the flexural energy (dashed line in Fig. 14) dramatically changes as a function of the thickness: for very low t values, almost all the impact energy just before delamination initiation is stored in flexure; on the contrary, when $t = 3.1$ mm or more the energy is mainly accumulated in the material volume close to the contact area.

It was possible to separate the energy at delamination initiation into two major contributions: one accounting for flexural deformation and the other for local deformation. The latter part becomes more and more important as far as the specimen thickness increases, so that it cannot be neglected for thick laminates.

3.4 Prediction of the Load Versus Displacement Curve

An important question to be answered in studying impact on composite laminates is the energy U_i required to cause first failure. In fact, while up to U_i the original material strength is retained, beyond this limit a residual strength being the lower the larger the imparted energy is.

In order to calculate the elastic energy stored in a plate at first failure, two conditions must be met: (a) the load-deflection curve must be described accurately;

(b) the critical force (or deflection) resulting in first failure must be evaluated correctly. The latter point was already successfully discussed. In what follows, the first topic will be treated and the equations for the prediction of U_i will be derived.

The study of the elastic response of composite structures is made intricate by many phenomena, among which the in-plane and along-the-thickness anisotropy are the most relevant. The bending-stretching coupling effects [61, 62], as well as the shear contribution to the deformation [63, 64], can considerably complicate the analytical development too. It was possible to simplify the study by introducing the fact that, when the impact velocity is low (up to 10 m/s), the static and dynamic response are similar [53–55], so that vibrational effects can be neglected and static tests can be adopted to simulate the impact behaviour. This assumption will be maintained along all this section, so that the vibratory effects will be disregarded. Nevertheless, in the first part of the impact phenomenon, before first failure occurs, the plate can be bent significantly and so, the non-linear effects deriving from the large deflections (thin laminates or large support diameter) become evident [65, 66]. When the tup displacement is adopted to find the load-deflection curve, the contact law must be included in the analysis.

Static tests simulating the dynamic ones and low velocity impact tests were carried out on anisotropic, simply supported and clamped circular plates made of graphite fibre reinforced plastic laminates of various thicknesses, 0.95, 1.90, 2.85 and 3.80 mm (TF in Table 1). According to $[(0, 90)_n/+45_n/-45_n]_s$ stacking sequence, n = 1 to 4, the plates were loaded at the centre by a hemispherical tup 12.7 mm in diameter. Two basic prepreg laminae, made of T400 fibres and HMF 934 epoxy resin, were used: in one, the fibres reinforcement was a plain weave fabric with a 193 g/m^2 in areal weight; in the other, the reinforcement was unidirectional with a 145 g/m^2 in areal weight.

The square plates 70 mm in side cut from the panels, were simply supported on a steel plate having a circular opening 50 mm in diameter. Some tests were stopped when sudden load drops were observed on the curve, clearly indicating significant damage development in the specimen; others were interrupted at predetermined load levels to investigate about the damage evolution.

3.4.1 Theory and Results

In performing both static and impact tests on composite plates, the tup displacement is often assumed to measure the plate deflection even if, in the case under study, the local deformation due to the contact between the indentor and the plate surface (Fig. 15) must be accounted for.

In Fig. 15, w_i is the local indentation, w_o the plate deflection and w_t the overall tup displacement given by the sum of w_i and w_o:

$$w_t = w_o + w_i \tag{18}$$

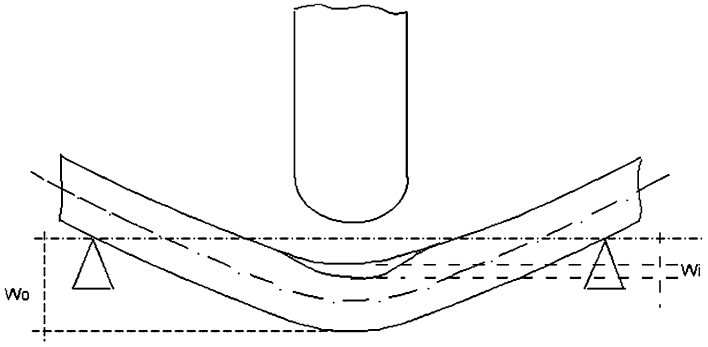

Fig. 15 Indentation due to the local contact tup-plate. w_i: local indentation; w_o: plate deflection

Simple strength-of-materials solutions are available in the literature, giving the deflection w_{ol} of circular isotropic plates subjected to small displacements. For instance, for a clamped plate loaded at the centre by a concentrated force F [16]:

$$w_{ol} = B \cdot \frac{F \cdot R^2}{E \cdot t^3} = \frac{F R^2}{16\pi D} \tag{19}$$

where R is the plate radius, $B = 1/16\pi$ a constant and $D = Et^3$ its flexural rigidity.

Unfortunately, the applicability of Eq. (19) to an anisotropic composite plate is not straightforward, since a laminate suffers the well known bending-stretching coupling effects [61, 62]. Moreover, the shear stresses arising along the thickness, whose effect is not taken into account in developing Eq. (19), can contribute considerably to w_{ol} [63, 64]. Finally, thin composite plates may be bent significantly before first failure occurs, overcoming the linear regime, within which Eq. (19) preserves its validity. The linear relationship between load and deflection, predicted by Eq. (19), is rapidly loosen with increasing the ratio of the deflection to the plate thickness, t. For sufficiently large values of this ratio, a higher-order theory, accounting for large displacements, must be addressed in order to accurately describe the elastic response of the structure [16]. Therefore, it is expected that, in general, w_o will not coincide with w_{ol}.

A closed-form, approximate solution for the large deflection of circular isotropic plates loaded at the centre is yielded in [16]:

$$\alpha D w_o + \beta E t w_o^3 = \frac{F R^2}{\pi} \tag{20}$$

α, β are two constants depending on the boundary conditions and E the elastic modulus of the material. In the case of clamped edge, $\alpha = 16$. The β value is strongly dependent on the possibility of the clamping device to prevent the radial displacement of the plate edge. If it is completely free, $\beta = 0.295$, whereas in the case of immovable edge $\beta = 0.650$ is readily obtained from the data in [16].

From Eqs. (19) and (20), it is easily to verify that $w_{ol} = w_o$ when the deflection is small, so that the cubic term on the left of Eq (20) is negligible compared to the linear one. The cubic term physically derives from the strain of the middle plane of the plate that is small when the deformation is small; as far as deformation increases, this phenomenon becomes more and more important and it must be accounted for in the analysis of large displacements.

Hoping that the validity of Eq. (20) could be retained at least for quasi-isotropic laminates exhibiting a moderate flexural anisotropy, its form was adopted in [67] as a starting point to model the load-displacement of composite plates. The E value in the equation, governing the stretching of the middle plane, was substituted by the in-plane modulus of the laminate. Recognizing that all the terms of the [D] matrix for a laminate can be expressed in the general form:

$$D = D_u t^3 \tag{21}$$

where D_u is representative of the flexural behaviour of the laminate, Eq. (20) was reduced to the following expression:

$$\frac{w_o}{t} + A\left(\frac{w_o}{t}\right)^3 = B\frac{F R^2}{E t^4} \tag{22}$$

with:

$$A = \frac{\beta E}{\alpha D_u} \tag{23}$$

$$B = \frac{1}{\pi\alpha} \tag{24}$$

From Eq. (18), also the local deformation w_i occurring at the tup-plate contact point must be known, if the overall displacement of the impactor is wanted. Rewriting Eq. (1) as a function of the local indentation [32]:

$$F = k_i (w_i)^{3/2} \tag{25}$$

useful in calculating the indentation w_i (Fig. 15).

In the field of small deflections, combining Eqs. (19), (18) and (25), the following relationship:

$$w_t = B \cdot \frac{F \cdot R^2}{E \cdot t^3} + \left(\frac{F}{k_i}\right)^{2/3} \tag{26}$$

is obtained. Equation (26) is valid only in the field of small displacements, since Eq. (19) suffers the same limitation.

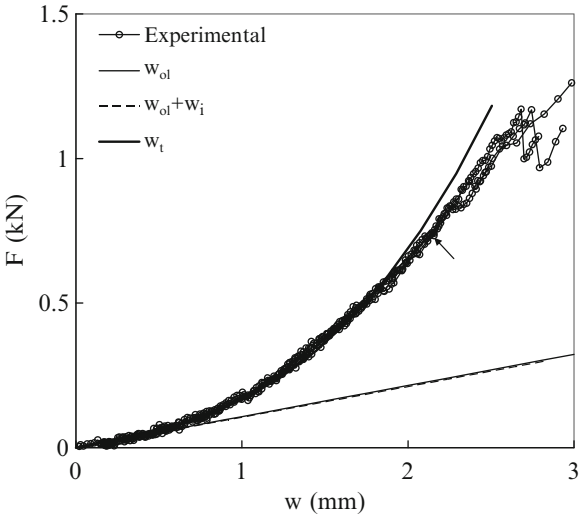

Fig. 16 Experimental load-deflection curves and theoretical predictions for the specimens with t = 0.95 mm

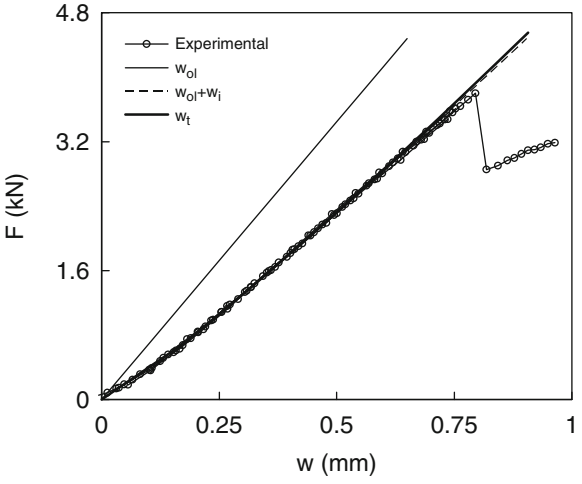

Fig. 17 Experimental load-deflection curves and theoretical predictions for the specimens with t = 3.80 mm

In Figs. 16 and 17, plots of the recorded load-displacement curves are shown for the lowest and the largest plate thickness tested, respectively. Apart some low-frequency oscillations, due to the dynamic effects, a divergence from the linear regime is observed in Fig. 16, with the plate rigidity increasing with increasing deformation. At a sufficiently high load (arrow in Fig. 16), high-frequency oscillations superpose to the fundamental frequency: this is a macroscopic effect of the first failures occurring in the laminate, revealed by the ultrasonic analysis, consisting of intralaminar cracks and delamination. Afterwards, both the load and the rigidity rise anew, until a clear load drop, denoting more pronounced failure phenomena, is recorded.

An increase in rigidity is present also in the first part of the curve in Fig. 17 even if, comparing Figs. 16 and 17, it is evident that the deviation from linearity is much more limited when a thick laminate is examined. This is expected from Eq. (22), according to which the effect of nonlinearity is more and more remarkable as the ratio of the deflection to the specimen thickness increases. Interestingly, it is confirmed that the first failure is much easier to detect from the load-displacement curve of the thick plate, resulting in a sharp load drop.

The continuous straight lines in Figs. 16 and 17 are the predictions of the load-deflection curves obtained on the basis of Eq. (19), i.e. simply assuming a linear behaviour without local indentation. Although the agreement between theory and experiments is good in the very early stage of loading in Fig. 16, the linear approximation results in an unacceptable error as soon as the deformation increases. Instead, for the thickest plate the theoretical prediction based on Eq. (19) results in a significant overestimation of the rigidity.

In order to assess the model presented, Eq. (25), to take into account the effect of non linearity, it is necessary to know the constants A and B/E in Eq. (22), and k_i in Eq. (25). To obtain B/E and k_i, use of Eq. (26) was made, together with an original method of data reduction, which was applied to the very early, linear portion of the load-displacement curve pertaining to $t = 3.80$ mm. The values $B/E = 1.27 \times 10^{-2}$ GPa^{-1} and $k_i = 34.9$ kN/mm$^{3/2}$ (C.V. $= 4.3\%$) were found here and adopted to evaluate $A = 0.56$ by best-fitting the load-displacement curve for $t = 1.90$ mm. The measured value of B/E was adopted in all the calculations hereafter. Some previous data, witnessing the physical consistency of the constants found, were recalled. In [32], values of k_i in the range 31.8–36.8 kN/mm$^{3/2}$, in excellent agreement with k_i evaluated here, were obtained. It was also shown that k_i is unaffected by the boundary conditions and specimen geometry, depending exclusively on the material and tup radius.

The dashed lines in Figs. 16 and 17 were drawn using the previous experimental values for B/E and k_i to calculate the quantity $(w_{ol} + w_i)$, even if they represent the predictions deriving from the hypotheses of linear elasticity and local indentation. Comparing these lines with the continuous straight ones previously discussed, it clearly emerges the role of local deformation w_i in determining the overall plate deflection. For the thinnest plates (Fig. 16), the two lines are practically coincident, indicating a negligible effect of the indentation whereas, the gap between the two curves increases with increasing the plate thickness. In Fig. 17, in fact for the laminate 3.80 mm thick the gap between the two curves is considerable. These results are qualitatively anticipated since large local deformations require high loads, which only thick plates can withstand without exceeding the elastic field.

However, from the comparison between Figs. 16 and 17, Eq. (26) tends to underestimate the force values for a fixed deflection value, with an error rapidly increasing with decreasing t resulting in an analytic solution unacceptably inaccurate for the thinnest plates (Fig. 16).

The thick solid curves in Figs. 16 and 17 represent the theoretical predictions from Eqs. (22) and (18), i.e. taking into account all the factors involved in the

deformation of the laminates. In the case of the 3.80 mm thick plates (Fig. 17), the non-linearity effect due to the cubic term in Eq. (22) is very small, as witnessed by the negligible difference between the dashed and the thick continuous curves. The influence of non-linearity increases with the decrease of the thickness, and it is very evident for the thinnest plate (Fig. 16). In any case, the load-deflection curve is modelled with great accuracy by theory as also confirmed by the data concerning the laminates of intermediate thicknesses, not shown here for brevity.

In conclusion, at this point it is possible to say that about the possibility to predict the first part of the load curve, for thin plates, the effect of indentation on the overall deflection can be neglected, whereas the cubic component in Eq. (22) plays a major role in determining the plate response; at the increasing of the thickness, the influence of the cubic component in Eq. (22) becomes lower and lower, whereas the effect of indentation on the deflection becomes relevant.

In what discussed above, generated under quasi-static conditions, demonstrated that Eq. (22) alone is not capable to efficiently describe the plate behaviour. The reason was found in the local indentation w_i occurring at the indentor-material contact point, which markedly affects the response of the structure, especially when large thicknesses are involved.

Three constants, A, B and k_i, were experimentally determined to solve the problem of the prediction of the elastic behaviour of a plate under dynamic conditions.

Further experimental support to the previous theoretical model was provided in subsequent works, where [67] the load-displacement curves deriving from both static and low-velocity impact tests on fabric laminates were predicted accurately. The possibility to reduce to two the number of unknown constants, yet achieving a reasonably good agreement between theory and experiments, was also discussed.

A modified version of the solution proposed above for quasi statically loaded tape laminates was developed in [67] for fabric laminae (F in Table 1) subjected to low-velocity impact. The formula (Eq. 22) was modified, to take into account the tup displacement associated with indentation. It is shown that the number of unknown constants can be reduced to two, yet achieving a good agreement between theory and experiments. Further, the relative importance of indentation and large displacements in affecting the load-displacement curve is assessed.

From the results, the analytical model accurately describes the actual elastic behaviour of the plates, provided two of the constants appearing in it are experimentally determined. The results discussed about thin and thick laminates were confirmed.

By the best fit method, the local rigidity $k_i = 12.0$ kN/mm$^{3/2}$ was obtained by Eq. (26) and from the curves recorded for the thickest plates. This value is about one third-one fourth compared with those found above and in [32, 68] for CFRP laminates made of tape laminae. This is due to the fabric architecture of the present composites, possibly playing a role in lowering k_i. The previous k_i was adopted as a constant independent of the laminate thickness [32].

Table 2 Plate thicknesses adopted for the various support diameters, D_s, and tup diameters, D_t

	D (mm)	
D_t (mm)	50	100
12.7	A	
14.9	1.90	
19.8	A	2.85

Legend: *A* All thicknesses

3.4.2 Influence of Support and Impactor Diameter. Development About First Failure Energy

Since the good results obtained for the prediction of the elastic part of the load curve, it is possible to proceed at the prediction of the elastic energy stored at first failure in a circular composite plate. The previous model is developed here to take explicitly into account the tup diameter, and is coupled with a previous formula [24] which is aimed at the prediction of the first failure load. From the two models, a formula for the calculation of the energy stored at first failure as a function of the test and material parameters is derived. Only when both the deflection at first failure and the tup diameter are large enough, the first failure load is significantly underestimated. The contribution of the different mechanisms of energy storage to the total energy at first failure is identified by the study of the analytical model. At the end, an analytical expression for the evaluation of the energy will be obtained.

The experimental tests were carried out on carbon fibre reinforced plastic laminates (FT in Table 1) of various thicknesses, which were simply supported at the periphery and loaded using two different supports, $D_s = 50$ mm and $D_s = 100$ mm, and three indentor diameters, $D_t = 12.7$ mm, 14.9 mm, and 19.8 mm. Table 2 shows the matrix of the experimental conditions adopted.

Some tests were stopped when sudden load drops were observed, others at predetermined load levels. After mechanical tests, each specimen was visually inspected and was then non-destructively evaluated by ultrasonic C-scan. Some of the samples were also sectioned, polished, and microscopically observed.

The results show that the elastic model, which takes into account the non-linearity due to the large displacements and the local indentation, is very accurate in shaping the load-deflection curve up to the first failure point. Also the predicted load and energy at first failure are in good agreement with the corresponding measured values. Both theory and experiments demonstrate that the critical load is independent of the support diameter in the range examined (50–100 mm), whereas it increases with increasing the plate thickness and the indentor diameter.

Comparing Eqs. (25) and (7), the influence of D_t on the local rigidity is clear:

$$k_i = \delta \cdot (D_t)^{1/2} \tag{27}$$

Knowing the k_i value for a given tup diameter, the corresponding local rigidity for another D_t value can be calculated.

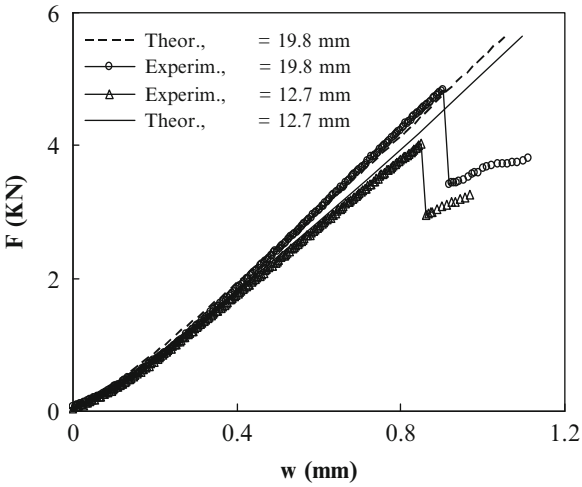

Fig. 18 Load-deflection curves for two different tup diameters, D_t. Plate thickness t = 3.80 mm. Support diameter D_s = 50 mm

For a given laminate and fixed boundary conditions, A and B/E will not change when the tup and support diameter are varied. k_i is a function of D_t through Eq. (27). Therefore, this equation can be used to calculate the appropriate value of the local rigidity for a given tup diameter, starting from k_i value found in the first part of this paragraph for the FT laminates of 34.9 kN/mm$^{3/2}$.

The effectiveness of Eq. (18) was already verified for different plate thicknesses. Hereafter the dependence of the elastic behaviour on D_s and D_t is estimated. Since the local rigidity was shown to be more evident when the flexural rigidity of the laminate is high, the support diameter $D_s = 50$ mm and the plate thickness t = 3.80 mm were adopted to verify the influence of the indentor diameter on the plate response.

From Fig. 18 (open symbols), the lower the tup diameter is, the lower the overall plate rigidity that is given by the rigidity of the plate plus the local rigidity, in qualitative agreement with Eq. (27).

The effect of the tup diameter within the range of D_t values considered is only moderate (Fig. 18). In the same figure, the theoretical predictions based on the analytical model are also plotted. The comparison between theory and experiments demonstrates an excellent agreement until the first failure point. The results obtained using Eq. (27) is interesting since some data was presented [32], showing that Eq. (27) does not model the effect of the tup diameter precisely.

The analytical prediction was successful used also to model the first part of the curve obtained using the support diameter $D_s = 100$ mm and tup diameter $D_t = 19.8$ mm. It is possible to conclude that the model is very accurate in describing the elastic behaviour of the laminate, accounting for the effect of thickness, as well as the influence of the support diameter and tup diameter.

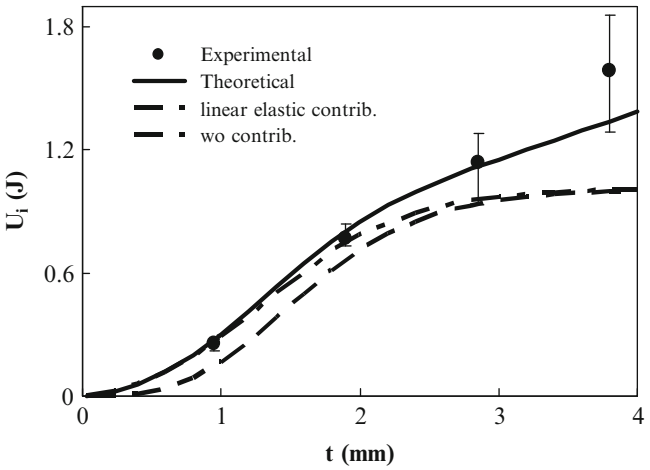

Fig. 19 First failure energy, U_i, against laminate thickness, t. Support diameter D = 50 mm; tup diameter D_t = 12.7 mm. Mat.: FT (Table 1)

Combining Eqs. (22), (25), and (9), and solving the integral, the following equation is obtained:

$$U_i = \frac{2 \cdot E \cdot w_o^{*2} \cdot t}{B \cdot D^2} \cdot \left(t^2 + A \cdot \frac{w_o^{*2}}{2} \right) + \frac{2 \cdot k_i \cdot w_i^{*5/2}}{5} \tag{28}$$

where the asterisk indicates the components of the deflection when $F = F_i$.

From Eq. (28), the first failure energy U_i as a function of the laminate thickness was calculated for the case D = 50 mm, D_t = 12.7 mm, and plotted (continuous line) in Fig. 19. The solid symbols are the experimental data, and show a very reasonable correlation with theory except for the thickest plates. In this case, the slight divergence of the actual trend from the expected one immediately before the load drop (Fig. 18) results in underestimating the actual energy storage capability of the material.

Looking at Fig. 19, the experimental data trend is well represented by a straight line but this should be misleading in the interpretation of the results in particular because the line does not pass through the origin, violating the boundary conditions.

The dashed line in Fig. 19 represents the energy associated with the linear elastic part of w_o, calculated through the analytical model. The dash-and-spot line is the portion of U_i due to w_o. Therefore, from the comparison of the two curves the effect of the cubic component of w_o on the stored energy is evidenced. As witnessed by the trend of the dash-and-spot and continuous line in Fig. 19, when high thicknesses are concerned, the importance of the energy correlated to the contact law cannot be neglected.

The model presented in Eq. (15) to explain the energy stored at first failure in fabric reinforced, quasi-isotropic CFRP laminates of different thicknesses, yielded consistent results. However, constant k_i values far lower than expected from

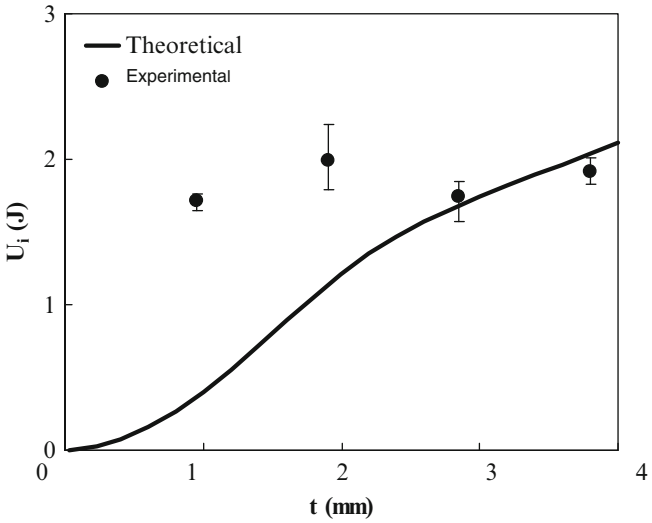

Fig. 20 First failure energy, U_i, against laminate thickness, t. Support diameter D = 50 mm; tup diameter D_t = 19.8 mm. Mat.: FT (Table 1)

previous works [32] were obtained through the energy data. The present results indicate that a reason for the poor correlation is the effect of non-linearity correlated with the cubic component of the deflection.

To add further confidence in the effectiveness of theory, the first failure energy for the case $D_s = 50$ mm, $D_t = 14.9$ mm was also evaluated through the present theoretical model. It was obtained $U_i = 0.91$ J, practically coincident with the measured value $U_i = 0.92$ J. The experimental results (symbols) and the analytical prediction (curve) of the first failure energy as a function of t for the case $D_s = 50$ mm, $D_t = 19.8$ mm are reported in Fig. 20. The agreement between theory and experiments is good only for a thickness $t \geq 2.85$ mm, whereas it is poor for the thinnest plates. This is not surprising, considering the effect of the plate curvature under loading on F_i, noted in Fig. 13. The interesting finding from Fig. 20 is that, especially when the plate is thin, the deformation can give a major contribution to its capacity of energy storage before first failure.

In Fig. 21, the influence of the support diameter on U_i is seen, where the data referring to a tup diameter $D_t = 19.8$ mm and $t = 2.85$ mm are also plotted as solid symbols, and the continuous line represents the corresponding prediction. Also in this case, the agreement between theoretical estimates and experimental results is satisfying. Of course, the increase in U_i with increasing D_s is due to the decrease in rigidity, together with the fact that the critical load remains the same, whichever D_s (Fig. 12).

For D_s values approaching zero, the accuracy of the present analytical model is expected to fail: in this case, the plate diameter becomes comparable with its thickness, so that the contribution of the shear deformation to the elastic behaviour, not considered here, becomes significant [33, 34].

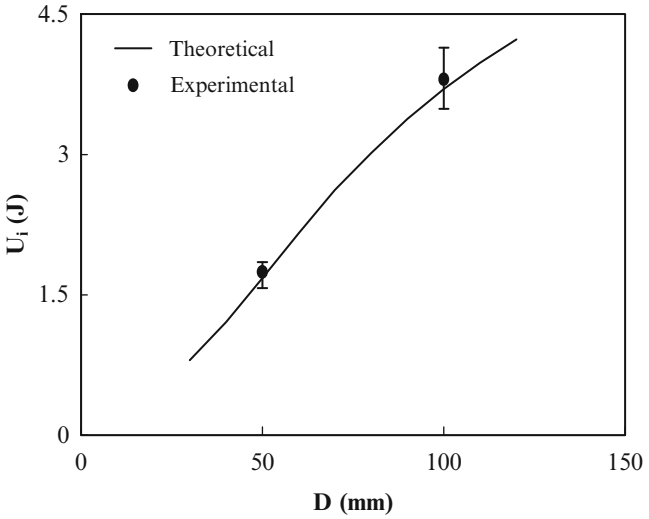

Fig. 21 Effect of the support diameter, D_s, on the first failure energy, U_i. Mat.: FT (Table 1)

According to Eq. (28), U_i is made of the sum of three terms associated with the linear and cubic components of the deflection and indentation, respectively. Consequently, the relative importance of the different mechanisms of energy storage at first failure can be appreciated if four constants, A and B/E in Eq. (22), k_i in Eq. (25), and δ in Eq. (7), are known.

The closed-form formula proposed and developed, aiming to predict the non-linear elastic behaviour of the plate, is successful in modelling the effect of both the support diameter and the indentor diameter on the elastic response. The first failure load is independent of the support diameter whereas it is a strong function of the tup diameter. Increasing the indentor diameter results in an increase in the critical load but this law is violated when the curvature caused by the applied load is significant compared to the indentor diameter.

3.4.3 Failure Energy of Glass-Fibre-Reinforced Plastic Panels

The above presented model was hereafter applied to predict the critical energy at first failure of simply supported circular glass-fibre-reinforced plastic laminates made of glass fabric/epoxy prepreg (G in Table 1). Four panel thicknesses, keeping the stacking sequence unchanged, and two tup diameters, $D_t = 16$ mm and $D_t = 19.8$ mm, were employed to verify the influence of these parameters on the elastic behaviour and first failure conditions of the material. Selected specimens was burnt away, and optical microscopy at low magnification was used to reveal possible reinforcement fracture. The experimental results were used to assess the same model proposed (Eq. 22) in the case of low velocity, large mass impact

on CFRP. The calculated values were in reasonably good agreement with their experimental counterparts. Only for the thickest laminate, the model yielded a far conservative estimate of the critical energy at first fibre failure, due to the deviation of the experimental load-displacement curve from the theoretical trend.

Through Eqs. (18), (22) and (25), the F-d curve is easily drawn: assigning a F value, w_o and w_i are calculated through Eqs. (22) and (25), respectively, then Eq. (18) gives w_t.

Accounting for Eqs. (18), (22), (25) and (7), Eq. (9) provided Eq. (28).

It is important to observe that Eq. (7), based on a stress approach rather than the more popular model proposed by Davies and Zhang [51]:

$$F_i = \pi \sqrt{\frac{8Et^3 G_{IIc}}{9(1-\nu^2)}} \tag{29}$$

deriving from energy considerations and successful in predicting delamination initiation for many quasi-isotropic laminates [51, 69, 70], was used in this work to calculate F_i. In Eq. (29), G_{IIc} is the Mode II delamination toughness, ν is the Poisson's ratio considered quasi-isotropic in the analytical development.

According to both Eqs. (7) and (29), F_i linearly increases with increasing $t^{3/2}$ whereas contrary to Eq. (29), Eq. (7) predicts a dependence of the threshold load on the tup diameter, not appearing from Eq. (29). Some experimental results supporting the increase of F_i with increasing D_t, in agreement with Eq. (7), were presented in [71].

In correspondence of the load drop in the force-displacement curve, fibre failure appeared at the back face of the laminate, as confirmed by optical microscopy after resin burning. Consequently, the load arrowed in Fig. 22 recorded for thin plates was attributed to fibre failure and is indicated by the symbol F_f hereafter.

In correspondence of the point signalled by the arrow in Fig. 23, obtained on thick plates, some irregularities, giving rise to a sawtooth appearance similar to the one observed in thin laminates, were noted. From visual analysis after tests, the knee signalling the departure from linearity was associated with delamination, and the abscissa of the corresponding load, F_d, was conventionally evaluated from the intercept of the two straight lines (dashed lines in Fig. 23) best fitting the approximately linear trend of the load-displacement curve before and beyond the knee, respectively. The maximum contact force preceding the sawtooth portion of the load-displacement curve (arrow in Fig. 23), associated with fibre failure, was also recorded.

Effect of Speed and Mass

The energy U in the impact tests was changed by varying not only the mass, but also the falling height (i.e. the tup velocity). This allowed to verify whether the parameters relevant to the impact phenomenon are rate-dependent or mass-dependent.

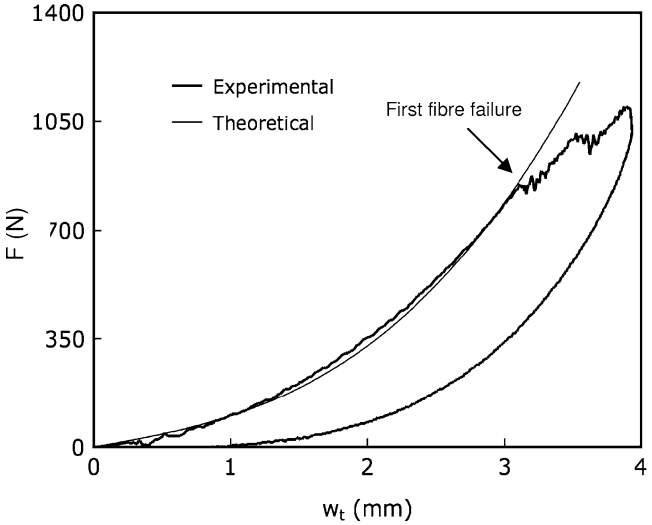

Fig. 22 Typical load-displacement curve recorded for the GFRP panels of thickness t = 0.96 mm. Indentor diameter D_t = 16 mm. Impact energy U = 1.68 J

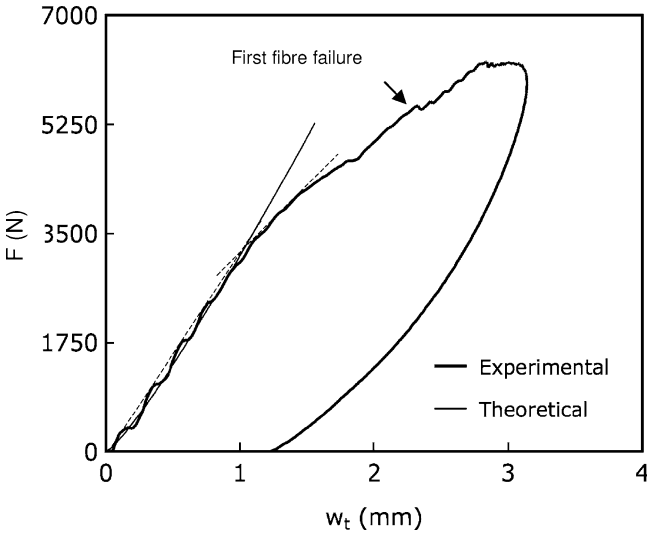

Fig. 23 Typical load-displacement curve recorded for the GFRP panels of thickness t = 3.84 mm. Indentor diameter D_t = 16 mm. Impact energy U = 12.2 J

Figure 24 shows the measured delamination load, F_d and the associated energy, U_d versus the impact energy, U, for t = 3.84 mm and D_t = 16 mm. They are, both, negligibly influenced by the impact energy and mass in the range adopted. The same was concluded by the examination of the shape of the overall F-d curves that is the same whichever the speed and mass.

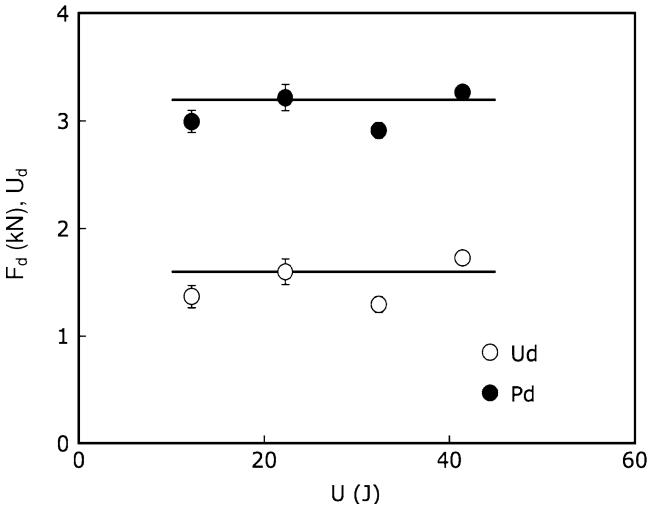

Fig. 24 Delamination load, F_d, and associated energy, U_d, against impact energy, U. Indentor diameter $D_t = 16$ mm. Panel thickness $t = 3.84$ mm

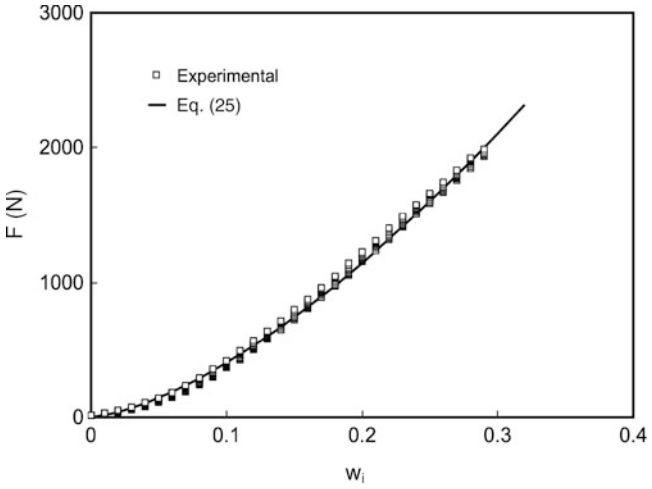

Fig. 25 Contact force, F, against indentation, w_i

To predict the load-displacement curve in the elastic phase through Eqs. (18), (22) and (25), the constants A, B/E, α must be known. As previously specified, α was directly measured through indentation tests, (results in Fig. 25). The solid line in Fig. 25 was drawn by Eq. (25), where $\alpha = 2.95$ KN/mm^2 was calculated by best fitting the experimental data. The good agreement between theory and experiments indicates that the contact law is effective in describing the phenomenon under study.

The values $A = 0.30$, $B/E = 1.73 \times 10^{-2}$ GPa^{-1} were obtained by a numerical technique based on the best-fit method, using the elastic portion of all the load-displacement curves. The A value is very near to that (0.27) valid for a simply supported, circular isotropic panel loaded at the centre [16] whereas it was previously found to hold 0.56, when CFRP laminates characterized by a low anisotropy ratio were tested. On the other hand, assuming $B = 0.55$ (isotropic materials), an unrealistically high E value, $E = 31.8$ GPa, larger than the elastic modulus (22–25 GPa) of the basic layer along the warp and weft directions, is calculated from B/E.

By substituting in Eqs. (18), (22) and (25) the values of the constants previously specified, the theoretical load-displacement curves were calculated and compared with the experimental ones (thin lines in Figs. 22 and 23). The correlation is outstanding at low displacements, indicating the effectiveness of the solution proposed in representing the elastic response of the panels. Beyond a given contact force, the experimental curves diverge from the calculated ones, denoting different damages.

According to theory, the effect of D_t on the overall shape of the elastic portion of the load curve is the more important, the thicker the laminate is. However, even for $t = 3.84$ mm, the effect of the tup diameter is hardly observable in the cases examined in this work: although not shown in Fig. 23 to avoid crowding of data, the thin line in the figure was hardly distinguishable from the one pertaining to $D_t = 19.8$ mm. It was confirmed by the results of the experimental tests.

Assessment of the Force Model

The open symbols in Fig. 26 are the measured F_d, whereas the full points in the same figure are the F_f values, plotted against panel thickness. Two different symbols have been used to distinguish the two impactor diameters, the vertical bars denote standard deviation. Both F_d and F_f increase steadily with increasing t and for a given t, a larger D_t results in a higher value of the first failure force.

From Eq. (7), the F_d data associated with the two tup diameters in Fig. 26 should converge to a single master curve, if the quantity $F_d/D_t^{0.5}$ is reported on the ordinate axis. In Fig. 27 the results in Fig. 26 have been rearranged according to this procedure: it shows that this actually occurs, supporting the effectiveness of Eq. (7) in modelling the influence of the tup diameter on F_d. More interestingly, the same law seems to be valid also for F_f. This result is not expected: the hypotheses on which Eq. (7) relies concern the distribution of the through-the-thickness shear stresses [10], which govern delamination initiation and propagation. The same assumptions are hardly acceptable for the normal stresses, responsible for fibre failure.

The solid and dashed lines in Fig. 27 graphically represent Eq. (7), in which the constant δ was calculated by best fitting the F_d and F_f data, respectively, obtaining $\delta = 105$ MPa (delamination) and $\delta = 200$ MPa (fibre failure). With these values in Eq. (7), the curves in Fig. 26 were drawn: they follow with sufficient accuracy the experimental results.

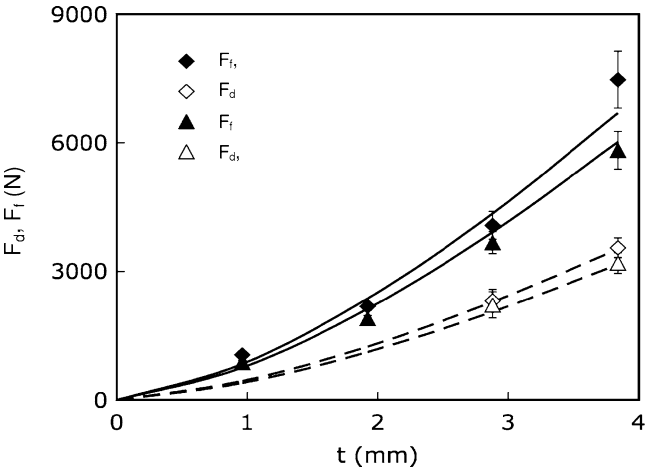

Fig. 26 Critical loads for delamination initiation, F_d, and fibre failure, F_f, vs panel thickness, t, for the two impactor diameters D_t used: open symbols $D_t = 16$ mm; full symbols $D_t = 19.8$ mm. Mat.: G (Table 1)

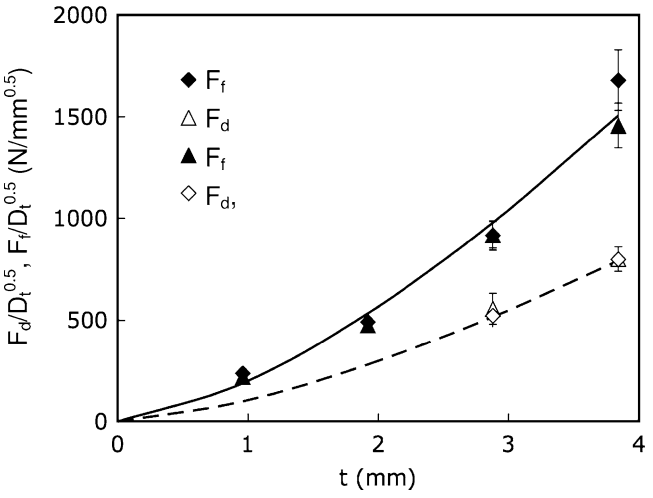

Fig. 27 $F_d/D_t^{0.5}$ and $F_f/D_t^{0.5}$ ratios versus panel thickness, t

First Failure Energy

The solid symbols in Fig. 28 represent the experimental energy at first fibre failure (yielded by the force-displacement curves in correspondence of F_f) against t for the two D_t adopted. The open symbols in the same figure are the energy U_d at delamination initiation. An increasing function of both laminate thickness and indentor diameter was found.

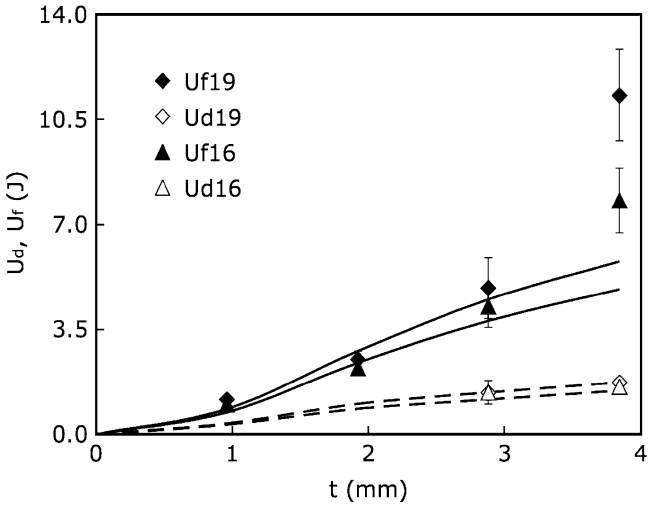

Fig. 28 Energies for delamination initiation, U_d, and first fibre failure, U_f, against panel thickness, t, for the two impactor diameters D_t used. open symbols $D_t = 16$ mm; full symbols $D_t = 19.8$ mm. Mat.: G (Table 1)

The curves in Fig. 28 were obtained by the theoretical predictions of the critical energies based on Eq. (28), in which the appropriate values of F_i ($F_i = F_d$, $F_i = F_f$) where inserted to obtain the corresponding energies ($U_i = U_d$, solid lines; $U_i = U_f$, dashed lines). The theory strongly underestimates U_f for $t = 3.84$ mm. It was anticipated, because of the knee in the load-displacement curves of the thickest panels, not taken into account by theory, bringing to an underestimation of the critical displacement at first fibre failure, w_f (Fig. 29). In the other cases, the theoretical model predicts with reasonable accuracy the experimental results also for the 2.88 mm thick panels, despite the existence of the knee in the load-displacement curve. The incongruence is explained by the fact that, as noted previously, the deviation from the theoretical elastic behaviour induced by delamination occurrence was negligible in this case.

From theory, the energy for delamination initiation in the 1.92 mm thick laminates is $U_d = 0.85$ J and $U_d = 1.01$ J for the two different impactors $D_t = 16$ mm and $D_t = 19.8$ mm, respectively. Unfortunately, impact tests at so low energy levels could not be carried out. Only a limited number of tests were performed setting $U \approx 1.5$ J using both the impactor diameters. Delaminated areas in the range 20–25 mm^2 were revealed by the visual inspections, whereas no evidence of fibre damage was yielded by the analysis after resin burning. This observation confirms that matrix damage is introduced in the material well before U_f is reached and the small extent of delamination suggests a stable growth, explaining the difficulty to individuate the occurrence of this mode of damage from the analysis of the load-displacement curve.

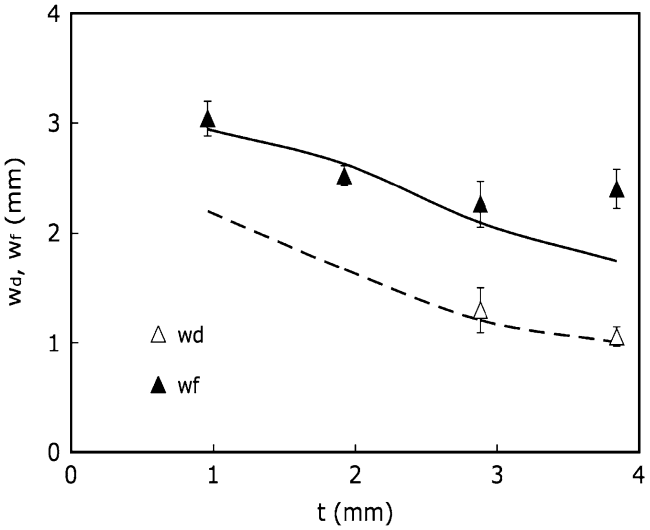

Fig. 29 Critical displacements at delamination initiation, w_d, and at first fibre failure, w_f, versus panel thickness, t. Tup diameter $D_t = 16$ mm. Curves: theoretical predictions

Final Considerations

A strategy suggested to easily determine the four constants appearing in the presented model (Eq. (22)) consists of two impact tests to be performed on a thick and a thin laminate, respectively. At low displacements, the cubic component of displacement for a thick laminate is negligible, while the effect of indentation is to take into account; these are the best conditions for measuring B/E and k_i from the load-displacement curve through the suggested procedure. On the contrary, the influence of indentation on the load curve of a thin laminate is insignificant whereas the membrane effect is evident, thus allowing for the evaluation of A. At the end, if the threshold load F_i is recorded from at least one of the two curves, also the constant δ is immediately obtained.

The present model does not account for the shear component of deflection, whose importance becomes more relevant the higher the ratios E/G (with G being the through-the-thickness shear modulus of the laminate) and t/D are, and the lower the indentor diameter is [52, 57]. The evaluation of the inaccuracy deriving from this approximation is not easy, because the shear stiffness is a function of contact area, which increases with the increasing of the applied load. To roughly estimate the maximum error made in the examined case, the data concerning the thickest panels and the lowest tup diameter were considered and the contact area pertaining to the maximum load experienced at the elastic limit was calculated through the equation provided in [12]. The shear and flexural stiffness were estimated, assuming typical values for the laminate elastic constants: the shear stiffness was found to be approximately ten times the flexural stiffness, resulting in a 9% error in the prediction of critical energy.

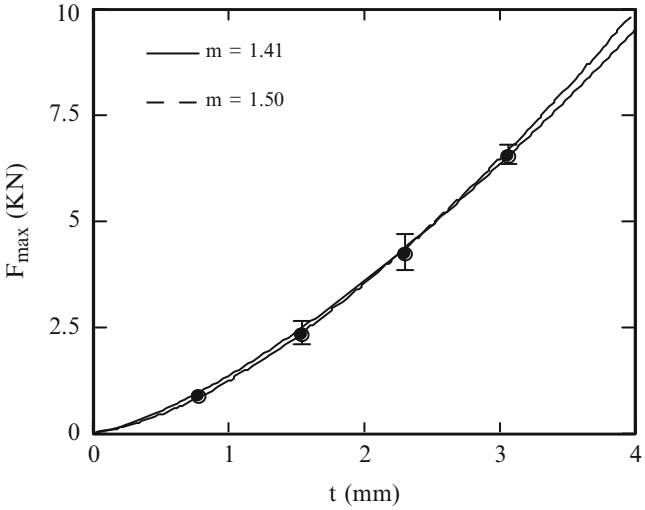

Fig. 30 Maximum contact force, F_{max}, against laminate thickness, t. Mat.: F (Table 1)

However, at the end, the discussed model is revealed to be able to accurately shape the elastic portion of the load-displacement curve, even when the laminate is so thin to exhibit an evident nonlinearity correlated with membrane effects It is able to predict the contact force corresponding to delamination initiation by a power law, in which a single parameter must be measured; the energy for delamination initiation, so that the energy at first fibre failure are well predicted by the model.

3.5 Maximum Force and Energy

The maximum contact force, F_{max}, could represent an important parameter in predicting the impact behaviour of composite laminates. Different authors [34, 72, 73], have noted that the failures in a laminate are force dependent rather than energy dependent. For this reason, it is necessary to understand how parameters such as specimen thickness can influence its value.

It was found that also F_{max}, follows a power law as a function of the thickness, with the exponent very similar to the exponent of the contact law. The same holds for the maximum energy, U_{max}.

In Fig. 30, the maximum load, F_{max}, measured on F carbon fibre laminates (Table 1) made of T400 fibres and HMF 934 epoxy resin, is plotted against the four specimen thickness, t, obtained with the following stacking sequence $\{[(0, 90)/(\pm 45)]s\}_n$ n = 1 to 4.

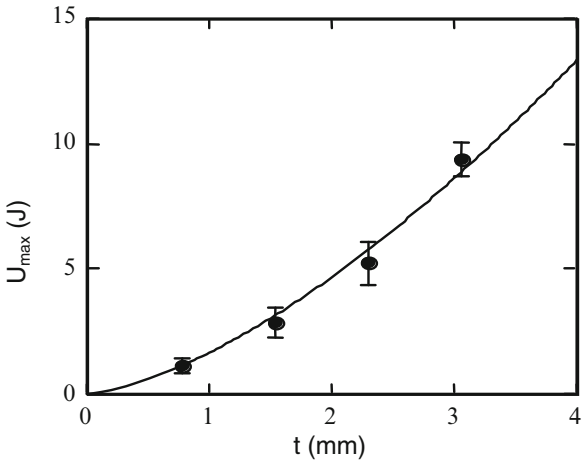

Fig. 31 Energy in correspondence of the maximum force, U_{max}, against laminate thickness, t

The continuous line is the best-fit power law, given by the equation:

$$F_{max} = F_{maxo} \cdot t^m \tag{30}$$

where $F_{maxo} = 1.35$ KN/mm^m, $m = 1.41$.

The values of the exponents i in Eq. (1) and m in Eq. (30) are very similar. This suggests that a strict correlation exists between the delamination initiation and the failure mechanisms resulting in the load drop just after the maximum force. If this is the case, the possibility to model F_{max} should critically depend on the ability to describe the first failure phenomena.

Also in Fig. 30 the experimental data were fitted by a power law having exponent 1.5 (dashed line), resulting in $F_{maxo} = 1.25$ KN/mm$^{1.5}$: the two curves are very close with each other. It could mean that, as already discussed about the first failure load, the importance of the contact law is deviced in determining the main laminate failure as well. There is in fact no difference in the prediction in adopting a power law having exponent 1.5.

The energy correlated to the maximum contact force presented above, U_{max}, was measured and plotted in Fig. 31 against the specimen thickness, t.

The continuous line in Fig. 31 is the best-fit power law having equation:

$$U_{max} = U_{maxo} \cdot t^n \tag{31}$$

with $U_{maxo} = 1.62$ J/mm^n, $n = 1.52$. Even the exponent n in Eq. (31), is very near to 1.5 that means that, considering Eqs. (30) and (31), an approximately linear correlation between the maximum force and the corresponding energy exists (Fig. 32).

In conclusion, the importance of the contact law is devised in determining the main laminate failure as well.

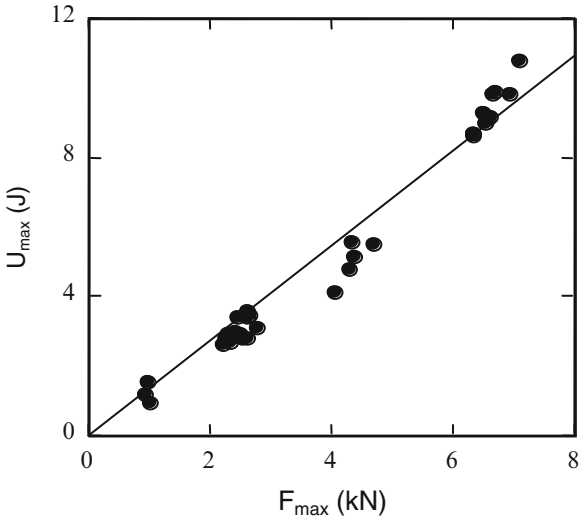

Fig. 32 Energy in correspondence of the maximum force, U_{max}, against maximum force, F_{max}

3.6 Indentation

With composite materials, it is difficult to detect impact damage by visual inspection even when considerable strength and rigidity losses have occurred. The external indication of an occurred impact is the indentation, the local deformation under the impactor the more pronounced the thicker the laminate is. It leads to the concept of 'barely visible impact damage' (BVID): at the aim to guarantee adequate safety, it is required an assigned minimum strength in the presence of a barely visible indentation generally fixed at 0.3 mm of depth. However, there is no common agreement on its value. This section considers the permanent indentation of laminated composites. In the development of mathematical models for the analysis of the impact dynamics, contact laws are needed to relate the dent depth to the impact energy and the residual strength to the dent depth.

After the impact tests carried out at different low energy levels when no perforation occurs, the specimens were taken away from the impact machine and a small permanent indentation depth, the only sign visible on the surface, was measured by a micrometrical dial gage. The measurements were carried out after the unloading phase of the impact tests when the impactor is not in contact with the material anymore and on the specimen there isn't any load. The indentation obtained in this way is the local permanent deformation due to the local contact load. Its trend was studied as a function of impact energy. The results obtained together with the experimental data available in the literature [65], were used to correlate the permanent indentation to the impact energy. A formula, modelling the residual tensile strength decay as a function of impact energy, is used to correctly predict the residual strength. Combining the indentation model and the residual strength model, a closed form model, explicitly correlating the residual strength and the indentation depth, is obtained.

Table 3 Details of the laminates tested in [65]

Material System	Symbol	Lay-up	Thickness (mm)	U_p (J)
T400 Fabric/934	F4	$[(0,90)/(\pm 45)]_s$	0.764	5.0
T400 Fabric/934	F8	$[(0,90)/(\pm 45)]_{2s}$	1.528	13.1
T400 Fabric/934	F12	$[(0,90)/(\pm 45)]_{3s}$	2.292	26.4
T400 Fabric/934	F16	$[(0,90)/(\pm 45)]_{4s}$	3.056	39.4
T400 Fabric/934 + SC[a]	SDF	$[(0,90)/(SC)/(0,90)/(SC)/(\pm 45)_2/(0,90)_2/(\pm 45)_2/(0,90)]$	3.751	29.9
T400 Fabric/934 + SC[a]	SEF	$[(0,90)/(SC)_2/(0,90)/(\pm 45)_2/(0,90)_2/(\pm 45)_2/(0,90)]$	3.751	30.1
T400 Fabric/934 + SC[a]	SIF	$[(0,90)/(\pm 45)_2/(0,90)/(SC)]_s$	3.560	18.9
AS-4 Tape/PEEK	A8	$(0/45/90/-45)_s$	1.056	19.2
AS-4 Tape/PEEK	A24	$(0/45/90/-45)_{3s}$	3.168	30.0

[a]SC = SynCore®

3.6.1 Relationship Between Dent Depth and Impact Energy

In [65] low velocity impact tests were carried out follow the same experimental methods used here on laminates different in thickness, lay-up, and material system (Table 3): some of the laminates were under sandwich form, obtained by the insertion of one of two layers of a syntactic foam (Syncore®), 1.016 mm in nominal thickness each one, at predetermined locations along the plate thickness. For the sandwiches, the impact happened on the first layer in Table 3, so that for SDF and SEF the foam was very near to the material-tup contact zone.

The measured indentation was plotted against U for all the laminates examined (Fabric (F) type, Sandwich (S) type, and AS-4 tape (A) type composites). The indentation rate was found to increase with increasing impact energy and for given energy and material system, the dent depth is the higher, the lower the plate thickness is. In Fig. 33, the results obtained on F laminates were reported for example.

SDF and SEF had approximately the same behaviour, different from what exhibit by SIF, when sufficiently high energy levels are adopted. The latter result was unexpected since, according to the contact law, a higher indentation should be expected from SDF and SEF sandwich plates, due to the presence of the unreinforced core near to the impact surface. However, the maximum indentation depth is comparable to the specimen thickness indicating extensive failure phenomena in the material. Therefore, the experimental test conditions in [65] involved contact forces well beyond the limit within which law can be reasonably applied. For a fixed impact energy, a higher indentation is found for F8 compared to SIF. The two systems were made by the same type and number of layers, except for the presence of core in the SIF structure so, the effect of core in preventing indentation is evident.

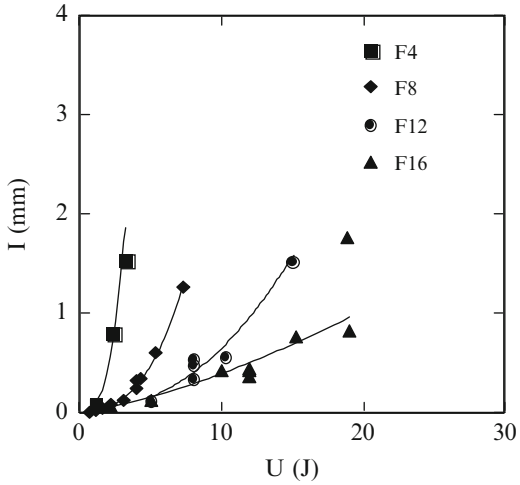

Fig. 33 Indentation, I, vs impact energy, U, for T400 fabric/934 laminates [65]. Mat.: F (Table 1)

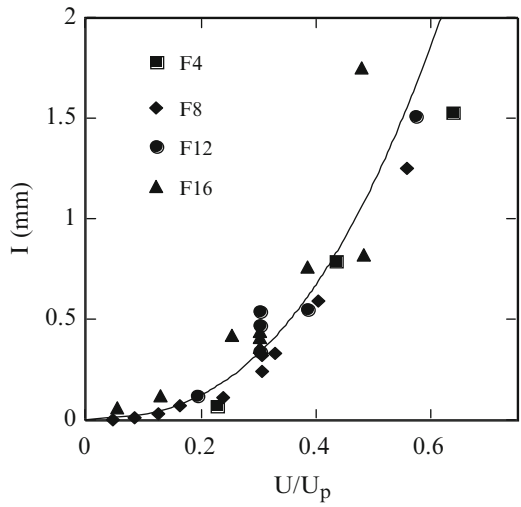

Fig. 34 Indentation, I, against non-dimensional impact energy, U/U_p (T400 fabric/934 laminates from [65])

In [65], the penetration energy U_p for all the laminates in Table 3 was evaluated (see last column in Table 3) as the area under the force-displacement curve up to the point in correspondence of which there is a marked decrease in slope and the cylindrical shaft supporting the tup hemispherical nose began to slide against the walls of the hole resulting from impact, dissipating energy by friction. In Fig. 34, the same data plotted in Fig. 33 are shown against the non-dimensional energy U/U_p. All the indentation data concerning a single material system, irrespective of the actual thickness, follow a master curve. It happens also for all the sandwich panels, despite the different location of the core, and the AS-4 tape (A) type system.

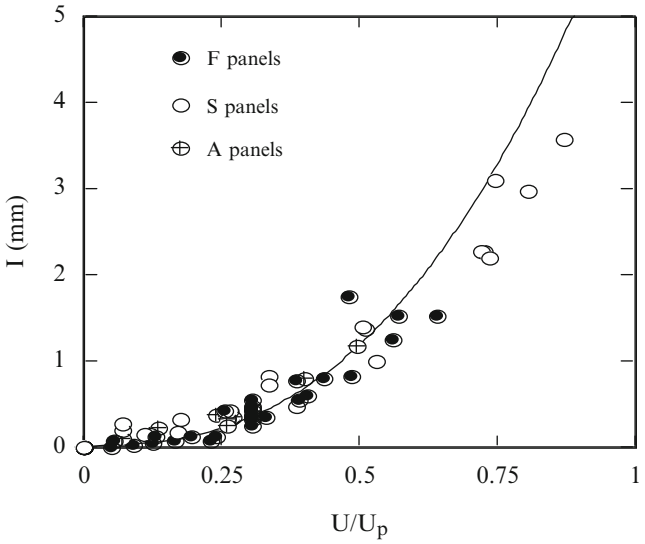

Fig. 35 Indentation depth, I, vs non-dimensional energy, U/U_p (Data from [65])

In Fig. 34, the power law equation:

$$I = I_o \cdot \left(\frac{U}{U_p}\right)^{\beta} \tag{32}$$

best fits all the F specimens experimental points, the values $I_o = 6.77$ mm and $\beta = 2.535$, resulting in the solid line in Fig. 34, were experimentally obtained.

In Fig. 35 all the indentation data of the material systems under attention are compared. It was found that the correlation between the data points and the curve found for the F type material is reasonable, demonstrating that the same equation can be used, independently of the actual material system, when an approximate evaluation of the non-dimensional energy is wanted. Equation (32) is very useful to calculate the impact energy from indentation measurement if the penetration energy U_p for a given laminate is known. However, looking better in Fig. 35, the agreement between theory and experimental trend is very good up to impact energy of about 60% of the penetration one. After that, the prediction overestimates the S panels behaviour.

Similarly to what above described about low-velocity impact, more data from quasi static tests on the same fabrics labeled as F4, F8, F12 and F16, were collected. It was also found that the rate of increase in indentation (Fig. 36) increases with the indentor energy and I strongly depends on the panel thickness, being the higher the thinner is the laminate, for a fixed energy level.

As already done previously, the data in Fig. 36 were then plotted against U/U_p (Fig. 37). As already observed for the dynamic case, all the points converge to a

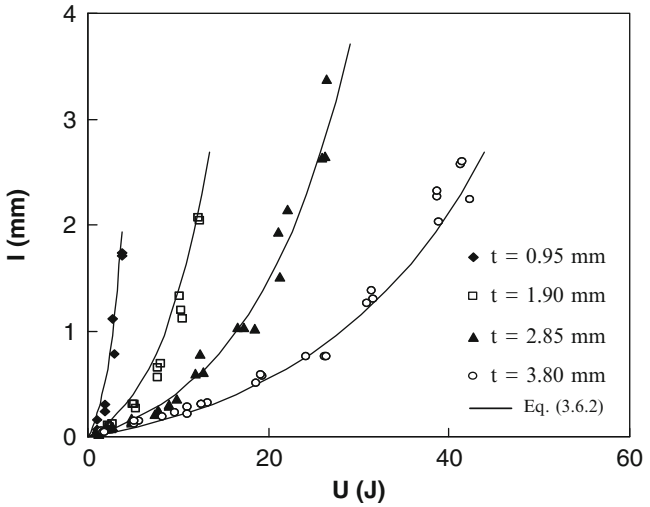

Fig. 36 Measured indentation, I, against impact energy, U

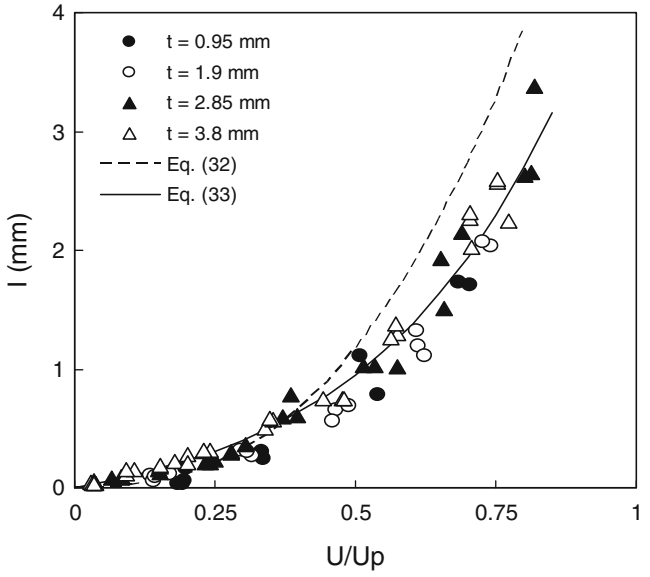

Fig. 37 Indentation, I, against non-dimensional energy, U/U_p

single master curve, indicating that the influence of the thickness disappears when the non-dimensional energy is used as the independent parameter.

The dashed line in Fig. 37, is the curve obtained from Eq. (32) best fitting the experimental data taken in [65] about impact tests carried out on T400/934 fabric laminates obtained above. Up to $U/U_p \cong 0.4$ the agreement is reasonable but

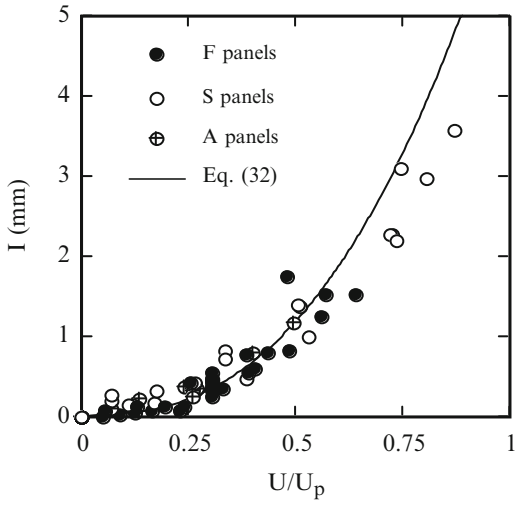

Fig. 38 Indentation, I, against non-dimensional energy, U/U_p, for the laminates from Table 3

the predicted indentation is higher than the measured values beyond this limit. To understand whether the discrepancy reflects the effect of loading speed, or material, or whether some other reason can be given to explain the phenomenon noted, in Fig. 38 the indentation data generated in [65] for the T400/934 fabric laminates (black circle), were reported. The best-fit curve calculated above and plotted in Fig. 37 (continuous line) is also shown in Fig. 38 for comparison purposes: a good fitting of the data was observed.

In Fig. 38 the data previously shown about the sandwich structures made of T400/934 fabric and Syncore® syntactic foam and the quasi-isotropic laminates made of AS-4 tape/PEEK are also reported. It was confirmed what discussed above about some deviation of that points giving the possibility to assert that the constants appearing in Eq. (32) could be mildly dependent on the specific material under examination.

All the points in Figs. 37 and 38 are collected in Fig. 39 where, contrary to what speculated above, a single indentation law actually holds for all the laminates considered, irrespective of the loading rate, fibre type and architecture, matrix type: once again, all the points converge to a single curve if plotted against the non dimensional energy, even if they showed different trends when plotted against the impact energy U since the dependence on the thickness and the particular material system. It seems that even the boundary conditions scarcely affect the relationship between I and U/U_p since the quite different constraint conditions previously adopted for the impact tests (plates clamped, support diameter 40 mm) from here where the plates were simply supported and the support diameter is 50 mm.

The dashed line in the figure represents the best-fit curve obtained calculating the constants appearing in Eq. (32) from all the points in Fig. 39. It is evident that again Eq. (32) is able to fit well the data up to about $U/U_p \cong 0.6$, beyond which it unacceptably underestimates indentation.

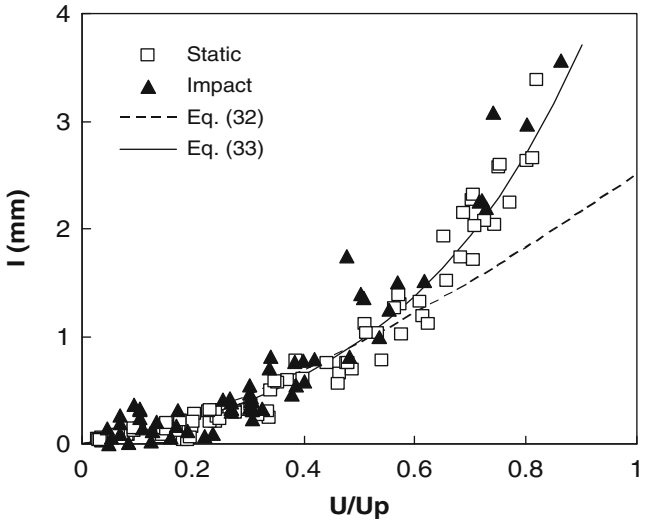

Fig. 39 Indentation, I, against non-dimensional energy, U/U_p, for both static and dynamic cases

The following expression, satisfying the boundary condition $U/U_p = 0 \Rightarrow I = 0$, was found to better correlate I and U/U_p:

$$I = k \cdot \left(10^{\gamma \cdot \frac{U}{Up}} - 1\right) \tag{33}$$

k, γ are two constants. From what here above asserted, these constants are expected to be negligibly affected by the particular laminate and matrix type.

Plotting Eq. (33) in a log scale (Fig. 40), it results in a straight line having slope γ useful to obtain the k value from the best fit method.

The k value was varied until the straight line best fitting the data passed through the origin. In this way, the values $k = 0.288$ mm and $\gamma = 1.269$ were obtained. The continuous lines in Figs. 36, 37, 39 and 40 were drown using Eq. (33): a good correlation between the new indentation model and the experimental data can be appreciated.

The most important conclusion is that, if U_p is known, the impact energy that cause a given indentation can be obtained from the measurement of the indentation depth. The found indentation law (Eq. 33) seems to have a quite general applicability, being scarcely affected by the fibre type and orientations, matrix type and clamping conditions.

Since the importance of the absorbed energy, U_a, in determining impact damage evolution, the same procedure applied above was followed considering U_a instead of the impact energy.

The impact energy, U, is related to the absorbed one, U_a through the penetration energy. In Fig. 41 the non dimensional value, U_a/U_p, is plotted against the ratio

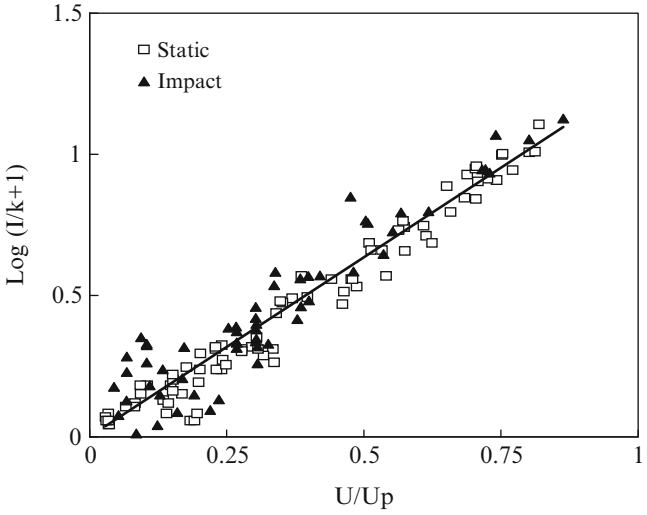

Fig. 40 Calculation of the constants in Eq. (33)

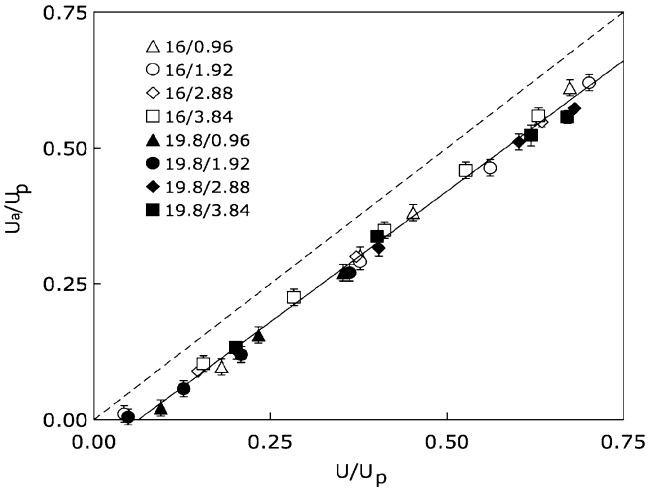

Fig. 41 Non dimensional absorbed energy, U_a/U_p, vs non dimensional impact energy, U/U_p. Mat.: G (Table 1)

U/U_p for E GFRP laminates, $[(0,90)_n/(+45,-45)_n/(+45,-45)_n/(0,90)_n]$, with $n = 1$ to 4: the vertical bars denote standard deviation and the symbols are identified by the label "A/B", where A stand for the tup diameter and B for the panel thickness in mm. All the data follow a single linear trend, irrespective of the panel thickness and impactor diameter. Only two points on the left at very low non-dimensional impact energy seems to have a deviation from linearity.

Sutherland and Guedes Soares in [74] observed a bi-linear trend between the absorbed energy plotted against the impact one, U, on GFRP laminates made of different woven roving architectures, thicknesses, and resins. They found a correspondence between the knee of the bilinear trend and the onset of fibre damage. The knee in the present case, should be located in the range $U/U_p = 0.08$ to 0.11.

Discarding the two points on the left, the solid best-fit straight line in Fig. 41 has equation:

$$\frac{U_a}{U_p} = 0.962\frac{U}{U_p} - 0.0609 \tag{34}$$

From the results, both the constants in Eq. (34) substantially hold whichever t and D_t. The virtual non-dimensional energy U_o/U_p corresponding to $U_a/U_p = 0$, represented by the intercept of the straight line with the x-axis, was calculated: $U_o/U_p = 0.063$. Therefore, would the linear relationship hold also at very low energy values, a perfect elastic impact should occur when the initial energy is about 6.3% or lower of the perforation one.

The dashed line in the same figure represents the condition for which all the available energy is absorbed and has equation $U_a/U_p = U/U_p$. Since the elastic portion of the non-dimensional impact energy, U_{el}/U_p, is given by $U_{el}/U_p = (U-U_a)/U_p$, the vertical distance of the generic experimental point from this line is given by U_{el}/U_p. With this in mind and considering that the slope of the continuous line is 0.962, very close to 1, it is possible to conclude that, beyond U_o, the elastic energy negligibly increases with increasing impact energy. U_e is nil at perforation that means that close to the perforation, the linear relationship in Fig. 41 will be violated.

At the increasing of impact energy, U, a part lower and lower of the initial energy is stored elastically, compared to the absorbed energy. This is clear in Fig. 42 where the data shown in Fig. 41 have been rearranged, plotting U_a/U against U/U_p. From Eq. (34) the following relationship for the solid line was obtained:

$$\frac{U_a}{U} = 0.962 - 0.0609\frac{U_p}{U} \tag{35}$$

From the figure it is clear that, at very low impact energy, a considerable portion of the impact energy is transferred back to the tup. Even when U is 25% of the perforation energy, about 71% of the energy is absorbed; at $U/U_p = 0.75$, only 12% of the energy is employed for rebound.

What above presented for glass fibre was done for carbon fibre reinforced plastic too.

In [74] the energy absorbed in low-velocity impact tests on GFRP laminates made of different woven roving architectures, thicknesses, and resins was plotted against U a linear trend similar to the one found here was observed for high values of the impact energy, U, whereas, at lower U a new straight line, with a lower slope,

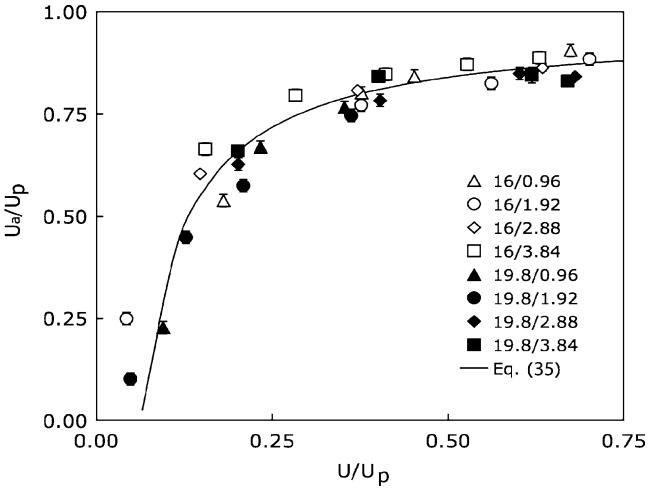

Fig. 42 Non dimensional absorbed energy, U_a/U_P, vs non dimensional impact energy, U/U_p

was necessary to effectively fit the experimental data. On the base of the analysis of the failure modes, the point of intersection of the two straight lines was found to coincide with the onset of fibre damage.

In a previous paper [24], low-velocity impact tests were carried out on CFRP T400/HMF 934 fabric laminates with the stacking sequence $\{[(0, 90)/(\pm 45)]_s\}_n$, with $n = 1$ to 4, and the thicknesses in the rang 0.76 and 3.01 mm with a hemispherical tup 12.7 mm in diameter. Some of the data from [24] were analyzed anew in this contest, the absorbed energy was evaluated, and its non-dimensional value U_a/U_p was plotted against U/U_p in Fig. 43. It is immediately clear in this figure the bi-linear trend highlighted by Sutherland and Guedes Soares [74], where the knee was associated with the onset of fibre damage. The latter would occur for $U \ 0.2U_p$ much earlier for the GFRP previously studied. The fact that in Fig. 43 the straight line fitting the data located beyond the knee seems to pass through the point (1,1) suggests that the linear trend is preserved until perforation.

Plotting the indentation depth values, I, against the absorbed impact energy, U_a, as already observed for impact energy, U, for a given energy, the dent depth increases monotonically with increasing U_a and it is the larger, the thinner is the panel and the lower is the tup diameter. The effectiveness of Eq. (33) in which the impact energy, U, is substituted by the absorbed energy, U_a, is really appreciated. The same indentation model previously presented (Eq. 33) assessed for the absorbed energy instead of the impact one, give the same good results. It was expected since the linear variation of U_a/U_p with U/U_p.

In Fig. 44, all the indentation data concerning GFRP (open triangles) and CFRP (full circles) are collected. Despite the scatter affecting the experimental data, it is obvious that GFRP laminates exhibit a larger indentation, for a fixed value of

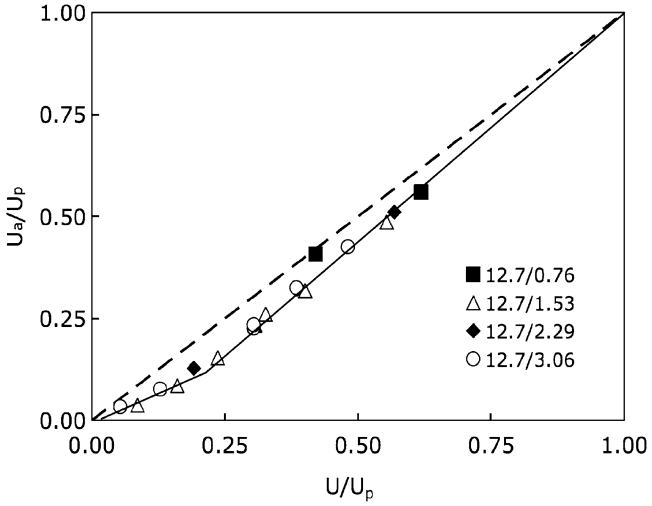

Fig. 43 Non dimensional absorbed energy, U_a/U_p, versus non dimensional impact energy, U/U_p. Material: CFRP [24]

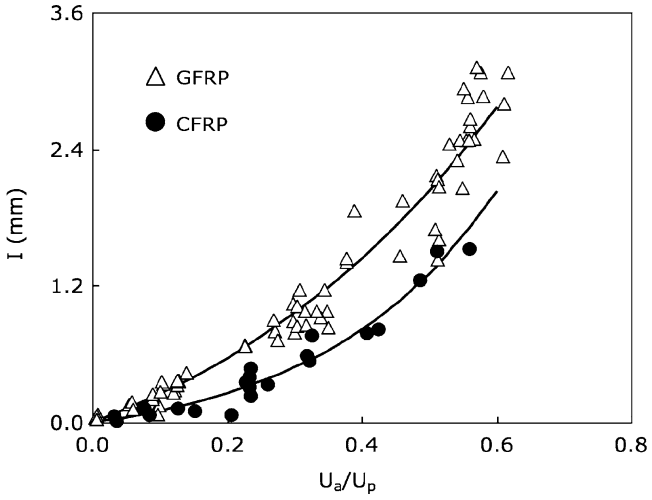

Fig. 44 Indentation, I, against non-dimensional absorbed energy, U_a/U_p, for CFPR (*full circle*) and GFRP (*open triangle*)

the non-dimensional absorbed energy. So, when the same indentation is measured on GFRP and CFRP systems, the latter absorbs a higher portion of energy, if the perforation energy is assumed as a benchmark.

The prediction model was revealed valid also considering U_a instead of U. In order to calculate the impact energy, U, or the absorbed one, U_a, from indentation measurements through Eq. (32) or (33), it is necessary to know the penetration energy, U_p, for a given laminate.

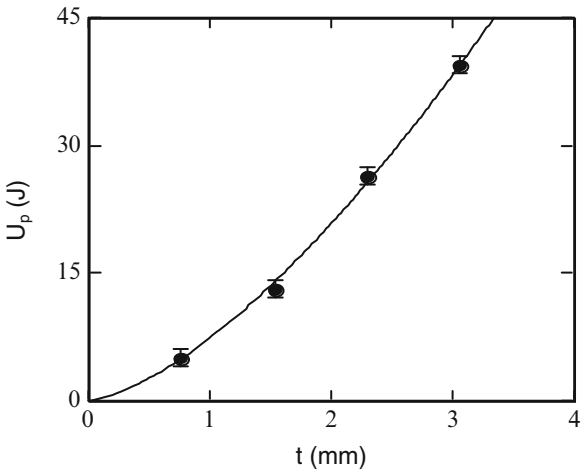

Fig. 45 Penetration energy, U_p, vs laminate thickness, t, for F laminates made of T400 fabric/934 layers [24]

3.7 Penetration Energy

This section deals with the prediction of the penetration energy, the difference between the initial and residual kinetic energy of the projectile during impacts resulting in complete perforation. The factors affecting the penetration energy of a composite material are examined.

For a given fibre type, the penetration energy is substantially influenced by the total fibre volume and tup diameter, whereas other factors, such as resin type and content, fibre architecture, stacking sequence and orientations, play a secondary role. An empirical power law equation proposed by the authors, is assessed on the basis of experimental results. Results indicate that the exponent of the power law is independent of the material considered, being practically the same for graphite fibre, as well as glass fibre reinforced plastics, and even for an isotropic material as polycarbonate, prone to extensive plastic yielding before final failure.

3.7.1 Effect of Laminate Thickness and Projectile Diameter

It is important to find a general formula to calculate the energy necessary to the indentor to completely perforate the laminate. The factors mainly affecting the energy under attention were first reviewed. In [23], the data in [24] for the F fabric laminates T400 fibres and HMF 934 epoxy resin having $\{[(0, 90)/(\pm 45)]_s\}_n$ stacking sequence, with n = 1 to 4, labelled as F in Table 1, were examined. The dependence of U_p on the laminate thickness is well described by the following power law:

$$U_p = U_{po} \cdot t^p \tag{36}$$

with $U_{po} = 7.33$ J/mm^p and p = 1.50, represented by the solid line in Fig. 45.

In [75, 76], the penetration energy for a given laminate was found to linearly increase with increasing t (i.e. fibre areal weight) but data from [17, 19, 21–23, 77] have demonstrated that doubling t or D_t results in more than doubling the energy absorbing capacity of the panel. So, the dependence for CFRP laminates could be well described by a power law having exponent 1.5 [17, 21]. Adopting the same law to fit the trend of data concerning GFRP [77], an exponent ≈1.35 was obtained.

However, before going on to develop the power dependence of U_p on t obtained with tests carried out in the present research, the experimental results obtained here together with data from the literature were utilized. The difficulty in comparing the various available data published derives from the fact that many factors, both internal and external, can affect the energy absorbing capacity of these materials. The most important ones are the matrix type and content, fibre type, architecture and orientation, laminate thickness and stacking sequence, the panel geometry and dimensions, the constraint conditions and the impactor geometry.

In [78], Babic and co-workers from the results of low-velocity impact tests on glass fibre reinforced plastics (GFRP) with different thicknesses and volume fraction of reinforcement, found that the scatter in the measured penetration energy was lower when U_p was plotted against the panel thickness, t, times fibre volume fraction, V_f, rather than against the actual thickness. The same was found in [22, 23], where different carbon fibre reinforced plastics and glass fibre reinforced plastics, were considered, respectively. The product $(t \times V_f)$ practically coincides with the total fibre thickness proportional to the total fibre areal weight, negligibly the void content. In [17], the authors obtained consistent results calculating U_p on the basis of the fibre areal weight alone. Therefore, what was found seems to indicate that the total fibre content plays a fundamental role in affecting the penetration energy and that not only the resin content, but also its type negligibly affects the penetration energy. In [22] six different types of resin were used to fabricate quasi-isotropic GFRP laminates subjected, then, to dynamic loads: very little differences in behaviour were observed. Bibo and Hogg [23] studied also the problem of the effect of fibre architecture on the penetration energy on quasi-isotropic laminates with different spatial distribution of reinforcement employing different forms of glass fibres (unidirectional, quadriaxial warp-knit fabric and eight-harness satin weave). For a fixed fibre areal weight, U_p revealed to be practically independent of the reinforcement architecture and stacking sequence although the delamination extent was quite limited in some cases and considerable in some others, indicating that the energy associated with delamination is negligible compared to the overall penetration energy.

The insensitivity of U_p to the fibre architecture was confirmed in [77], where the energy absorbing capability of an in-plane isotropic sheet-moulding compound was shown to be the same as that of fabric laminates with the same fibre areal weight. This confirms the importance of the total fibre content and in addition supports the hypothesis that fibre orientation play a secondary role in determining the penetration response of a composite, at least when the anisotropy ratio is not too high like for quasi-isotropic laminates. This hypothesis is confirmed in [21], where Delfosse and Poursartip used different indenter diameters on two types of

graphite/epoxy laminates. The first one was quasi-isotropic, whereas the second had 40% of the fibres oriented in the 0-direction. The penetration energy increases with increasing the impactor diameter but for a given indenter diameter, the two composites exhibited the same U_p value. This indicates that, at least when the anisotropy ratio is not too high, also the fibre orientations play a secondary role affecting the penetration energy of a laminate and the main parameters remain the fibre type and areal weight.

Moreover, the penetration energy of $(\pm 30)_{2s}$, and $(\pm 45)_{2s}$ tape CFRP laminates was successfully calculated on the basis of the test results deriving from quasi-isotropic fabric laminates taking into account only the total fibre thickness and not the fibre orientation.

In [53], penetration tests were carried out on different forms of glass fibres (unidirectional, non-crimp fabric and eight-harness satin) utilised to fabricate quasi-isotropic laminates with different spatial distribution of reinforcement. The results demonstrated that the penetration energy is scarcely affected by the reinforcement architecture and spatial distribution, if the total fibre volume remains unchanged.

The dependence of U_p on D_t is not so clear yet. In [21], where some data concerning CFRP were presented, it was concluded that a power law having exponent 0.7 could be adequate to describe the trend of CFRP but completely different conclusions were highlighted in [77], where the power law best fitting the experimental points had exponent 1.38 for GFRP. Taking into account the latter case, it was noted that the effect of both the thickness and the impactor diameter on the penetration energy could be modelled by power laws having very similar exponents.

The results suggest that the parameter controlling the penetration energy is the product $(t \cdot D_t)$.

The reinforcement plays a major role in determining the impact response also for GFRP. In [78], in fact, the U_p of all the data about GFRP deriving from specimens having different matrix content converge to a single master curve when plotted against the total fibre thickness obtained as the thickness times fibre volume fraction. Looking at what obtained by the authors [77], the quantity $(t \cdot V_f \cdot D_t)$ seems to be a parameter useful to compare on a common basis data obtained on GFRPs with different resin contents and different impactor diameters. To demonstrate what asserted, the penetration energy data generated on GFRP recalled above and described in the materials paragraph, are plotted against $(t \cdot V_f \cdot D_t)$ in Fig. 46. Despite the differences in fibre architecture and orientations, the data about three different materials tested approximately follow the same curve, confirming the conclusions in [78], where the negligible importance of the matrix on the energy absorption capacity of GFRP was noted.

The power law in Fig. 46 has equation:

$$U_p = K \cdot \left(t \cdot V_f \cdot D_t\right)^{\alpha} \tag{37}$$

and with $K = 0.90$ and $\alpha = 1.30$ is useful in calculating the penetration energy of a glass fibre reinforced plastic, irrespective of the fibre architecture and orientations,

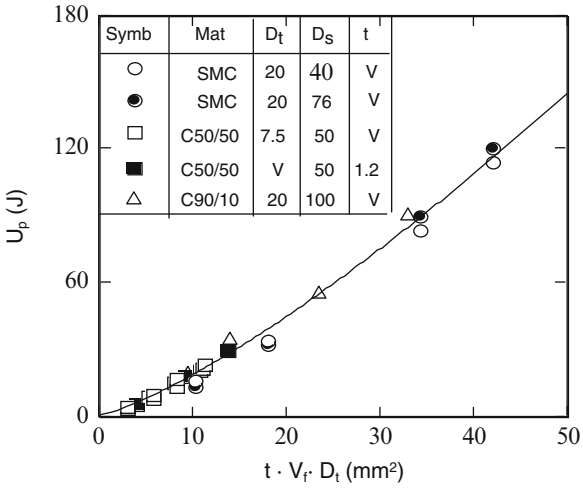

Fig. 46 Penetration energy, U_p, versus total fibre thickness times tup diameter, $t \cdot V_f \cdot \cdot D_t$. Table: dimensions in mm; D_s = support diameter; V = variable

and resin type. By examining the effect of each variable separately, it was found that U_p varied as a power function of each variable, the exponent being nearly the same. This suggested that U_p varies as in Eq. (37) where K and α are two experimental constant. The α value was found approximately equal to 1.3 independently of the examined variable.

This relationship is expected to be valid only for quasi-isotropic laminates and, as in the present case, the elastic energy stored in the structure is negligible compared to the energy expended in penetrating the material.

To demonstrate that relatively small variations in the matrix content do not affect considerably the penetration energy [23, 78], Eq. (36) can be expressed in the following form:

$$U_p = U_{po}^* \cdot W^p \tag{38}$$

where U_{po}* and p are two constant and W designates the total areal weight of fibre (proportional to the total fibre thickness), that is useful if the penetration response of laminates different in matrix content must be compared. In Fig. 47, the data of penetration energy measured on SDF, SEF, SIF and A laminates reported in Table 3, were plotted against W.

Plotting the F type laminates data from Table 3 showed in Fig. 45, as a function of W, by the best-fit power law the value $U_{po}^* = 7.22$ (valid when W is expressed in Kg/m^2) was found (Fig. 45) and used to draw the solid line in Fig. 47. As expected, S type and A type laminates follow a different trend respect to the F laminates ones and the AS-4/PEEK system seems to be less efficient than T400/934 in preventing penetration whereas, interestingly, the sandwiches showed a better impact response, for a given fibre areal weight. The latter demonstrates that the constants in Eq. (38) must be appropriately evaluated when sandwich structures are considered.

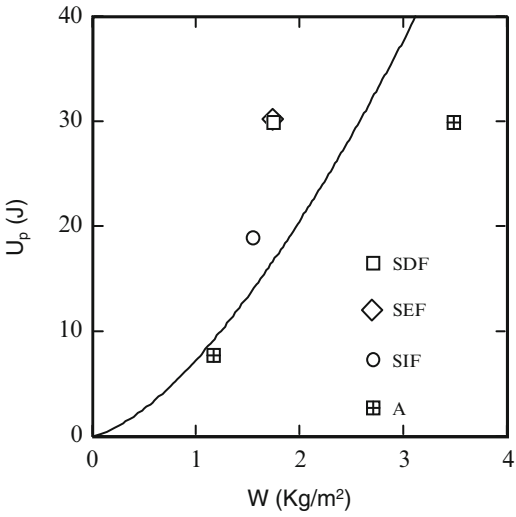

Fig. 47 Penetration energy, U_p, against fibre areal weight, W, for different laminates examined in [65]

The indentation law previously discussed (Eq. (32)) was used to demonstrate that the continuous line drown in Fig. 47 should be valid for a wide class of laminates based on the T400/934 system. Considering the Eq. (38) the following relationship was obtained:

$$I = I_o \left(\frac{U}{U_{op}^* \cdot W^p} \right)^{\beta} \tag{39}$$

in which the constants found for T400 fabric/934 are used to calculate the indentation as a function of impact energy for the $(\pm 30)_{2s}$, $(\pm 60)_{2s}$, and $(\pm 45)_{2s}$ laminates tested, made of T400 tape/934. The comparison between theory and experiments is carried out in Fig. 48, and the correlation between the experimental data and theoretical predictions is outstanding, whichever the actual laminate considered. This supports the idea that the constants in Eq. (38) are independent of both reinforcement architecture and fibre orientations.

In Table 4, a sufficiently large variety of carbon fibres (in Table 5 the mechanical properties are reported), matrix types, laminate lay-ups and thicknesses, constraint conditions, and penetrator diameters is covered. The support type is specified in the sixth column, through the code Annn/D, where "A" is the type of support (B = beam, Φ = circular plate, S = square plate), "nnn" is a number indicating the support dimensions, in mm (for beams, the length), and "D" is the type of constraint (S = simply supported, C = clamped).

The data presented indicate that the proposed formula has a quite wide applicability and can be probably further simplified, allowing a simple comparison of different materials.

In Fig. 49, in fact, the dependence on the total fibre thickness of all the laminates in Table 4 is shown on a log-log scale and results in a linear trend which slope

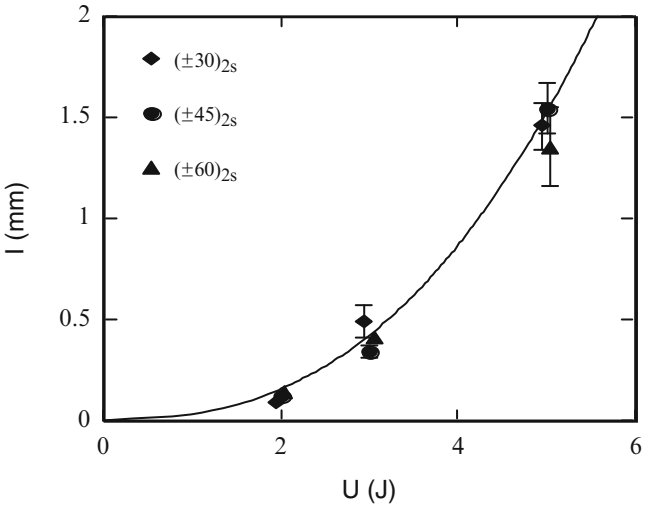

Fig. 48 Indentation, I, vs impact energy, U, for $(\pm\theta)_{2s}$ laminates made of T400 tape/934

Table 4 Carbon fibre reinforced plastic laminates tested at penetration

Ref.	Symb.	Material	Lay-up	t (mm)	Support	D_t (mm)
[18]	■	XAS/Epoxy, Tape	$(\pm45)_{ns}$	0.5 ÷ 4	B50/S	6
	♦	XAS/Epoxy, Tape	$(0, \pm45)_{ns}$	1.0 ÷ 2.0	B50/S	6
	●	XAS/Epoxy, Tape	$(\pm45)_{ns}$	0.5 ÷ 2.0	Φ120/C	6
[21]	◪	AS4/PEEK/LC[a], Tape	$(-45/0/45/90)_{ns}$	1.0 ÷ 3.0	Φ40/C	20
	◭	AS4/PEEK/HC[b], Tape	$(-45/0/45/90)_{ns}$	1.0 ÷ 3.0	Φ40/C	20
	◩	AS4/PPS/LC, Tape	$(-45/0/45/90)_{ns}$	1.0 ÷ 3.0	Φ40/C	20
	◹	AS4/PPS/HC, Tape	$(-45/0/45/90)_{ns}$	1.0 ÷ 3.0	Φ40/C	20
	◆	T650/PPS/Radel, Tape	$(-45/0/45/90)_{ns}$	2.0	Φ40/C	20
	◆	T800H/Epoxy, Tape	$(-45/0/45/90)_{ns}$	2.0	Φ40/C	20
[52]	□	T400/Epoxy, Fabric	0, ±45, 90	0.8 ÷ 3.1	Φ40/S	12.7
[57]	◇	AS4/Epoxy, Tape	$(0/90)_{5s}$	3.0	S127/S	12.7
	○	AS4/Epoxy, Fabric	$(0, 90)_{10s}$	2.2	S127/S	12.7
[58]	△	IM7/Epoxy, Tape	$[(0/90)_{22}0]_s$	6.4	Φ76/C	12.7
	⊞	IM7/Epoxy, Tape	$(90/\pm45/0)_{6s}$	6.8	Φ76/C	12.7
	◈	IM7/Epoxy, Tape	$[(0/45/90/-45)_{s2}/0/45/90]_s$	6.6	Φ76/C	12.7
	⊕	IM7/Epoxy, Tape	$[(0_2/\pm45)_{s2}/0_2/+45/-45_2/+45]_s$	6.4	Φ76/C	12.7
	▽	IM7/Epoxy, Tape	$[(02/\pm45)_{s2}/\pm45/0]_s$	6.5	Φ76/C	12.7
	▷	IM7/Epoxy, Fabric	$[(0/45)_9/45]_s$	6.4	Φ76/C	12.7

Legend: [a]*LC* low crystallinity [b]*HC* high crystallinity

Table 5 Mechanical properties of the fibre

Type	Modulus (GPa)	Strength (GPa)	Elongation (%)
XAS	234	***	***
AS4	221	4.0	1.6
T650	290	5.0	1.7
T800	294	5.5	1.9
T400	254	4.5	1.8
IM7	276	5.4	1.8

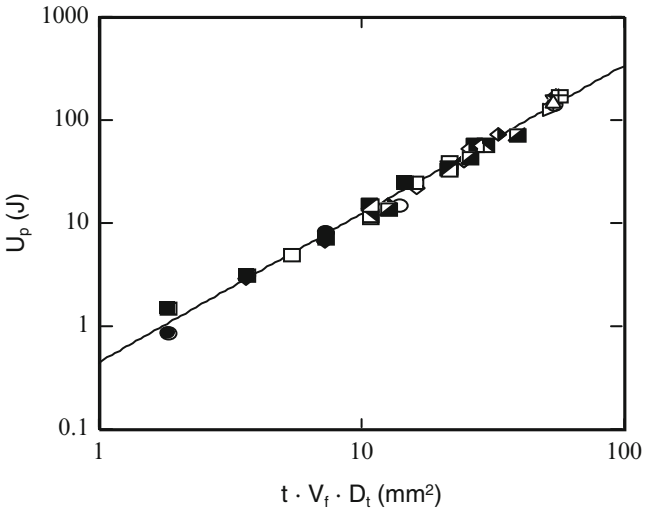

Fig. 49 Log-log plot of the penetration energy, U_p, vs $(t \cdot V_f \cdot D_t)$

(continuous lines each one for each different tup diameter) is unaffected by the particular D_t value. This is in agreement with Eq. (37), assuming a power law relationship between U_p and fibre thickness, and an exponent α dependent just on the material.

The values of the constants were found by the best–fit method providing $K = 0.45$ J/mm$^{2\alpha}$ and $\alpha = 1.44$ (continuous line in Fig. 49).

However, the analysis of the graph on a linear scale (Fig. 50) revealed an underestimating of the energy absorbing capacity at high values of the abscissa.

Also in [79], where a penetration model was developed in order to predict U_p as a function of the target thickness and specimen dimensions, a good agreement between theory and experiments was found up to 4 mm of thickness whereas the agreement was poor when an 8 mm thick laminate was considered. From microscopic observations of the failure modes during penetration and the energy associated with each ones or drawn from the literature, by sectioning and polishing the thick specimens, a substantial difference in failure modes was found between thin and thick laminates. Probably the validity of the model fails when thick composites were considered.

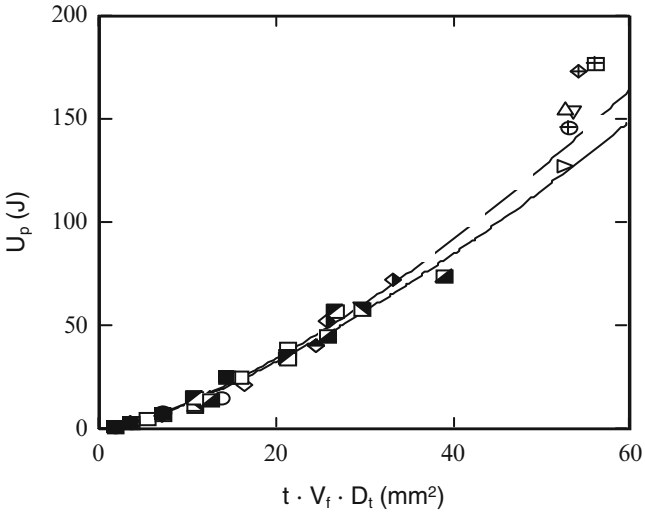

Fig. 50 Linear plot of the penetration energy, U_p, vs ($t \cdot V_f \cdot D_t$)

Here, it is not possible to know if high values of the abscissa are correlated with large tup diameters or thick laminates. However, all the points characterised by a high ($t \cdot V_f \cdot D_t$) value are about laminates of about 6.5 mm thickness and a change in failure modes can possibly explain the poor correlation between theory and experiments. The hypothesis is strengthened by the fact that, similarly to what found by Cantwell and Morton [79], also Eq. (37) tends to underestimate the penetration energy when the laminate thickness is high.

The values of the constants in Eq. (37) were, so, calculated anew only for the points characterised by ($t \cdot V_f \cdot D_t$) values lower than 40 mm^2, and 0.49 and 1.40 were found for K and α respectively. They are represented by the dashed line in Fig. 50.

The same was done on other material systems (GFRP and PC) and the similar results lead to the possibility to assume a single α value to describe the penetration energy trend. In this way, it could be simple to applied Eq. (37) since the parameter K could be used to rank different materials on the basis of their energy absorbing capacity provided the anisotropy ratio is not too high. The latter limitation is due to the fact that 0° composites are prone to transverse intralaminar failures, which can alter significantly the mechanisms of energy absorption under impact.

In Fig. 51 the best-fit straight line obtained for GFRP data discussed above is reported on a log-log scale together with the dashed line from Fig. 50 to allow a direct comparison of the energy absorbing capacity of GFRP and CFRP: glass fibres are superior with respect to graphite fibres even if the two straight lines tend to cross each other at high ($t \cdot V_f \cdot D_t$) values. The latter denote a better behaviour of CFRP when large tup diameters are used. The crossover point is well beyond the range of the experimental points available and it is a result of extrapolation. Since it

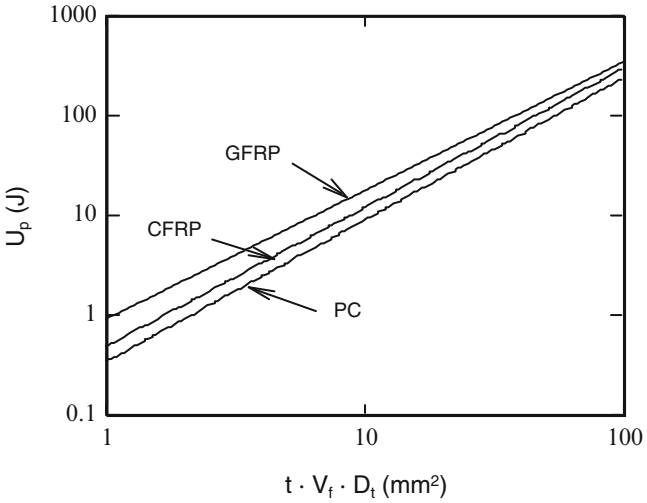

Fig. 51 Comparison of the energy absorbing capacity

is not clear whether the difference in α values between CFRP and GFRP is actually significant or it is only due to the data scatter, additional experimental data will be hereafter discussed, indicating that Eq. (37) can be possibly applied to a large class of materials and further simplified in form.

In [80], low velocity impact tests were performed on polycarbonate (PC) and GFRP panels supported on circular rings, and the influence of panel thickness and penetrator diameter on the penetration energy was examined. The energy absorption modalities were very different: in GFRP, in fact, as usually found in the literature for composite materials [21, 65, 75, 80–82], most of the energy was associated with the propagation of failure phenomena taking place beyond the onset of damage. On the contrary, PC exhibited an extensive permanent indentation, exclusively responsible for energy absorption. The energy associated with crack propagation after the maximum load was negligible: a fast propagation of cracks generated in correspondence of the contact point was observed witnessed by the sudden drop in the contact force down to zero.

The same procedure presented above was repeated for PC considering the measured panel thickness instead of the product $t \cdot V_f$. Once again the validity of Eq. (37) was clear, despite the marked differences in the mechanisms of energy absorption between PC and composites: the superposition of the points referring to different thicknesses and different tup diameters was very satisfactory.

The values of the constants K and α were calculated as previously done also for PC, obtaining $K = 0.35$ J/mm$^{2\alpha}$ and $\alpha = 1.42$. The continuous, best-fit straight line obtained for PC was reported in Fig. 51 for comparison purposes and the values of the constants calculated for the three materials considered in this paper are collected in Table 6.

Table 6 Values of the constants in Eq. (37)

Material	K (J/mm$^{2\alpha}$)	α
CFRP	0.49	1.40
GFRP	0.90	1.30
PC	0.35	1.42

Table 7 Values of the constants K best fitting the experimental results for given values for α

Material	α	K (J/mm$^{2\alpha}$)
CFRP	1.30	0.67
	1.42	0.45
GFRP	1.30	0.90
	1.42	0.59
PC	1.30	0.56
	1.42	0.35

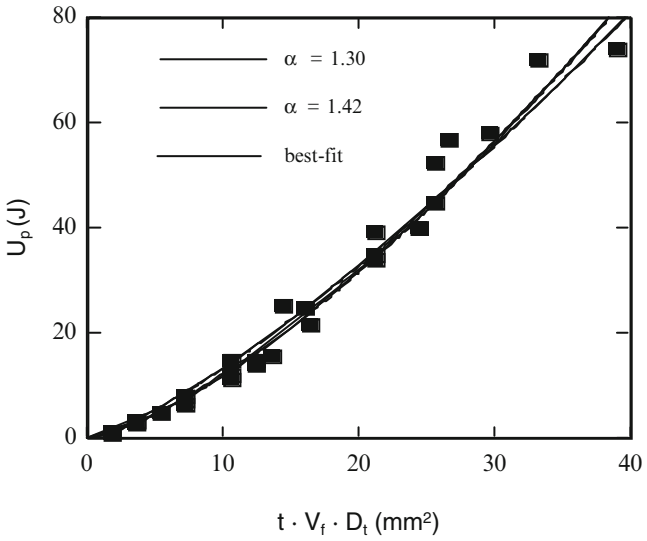

Fig. 52 Effect of the α value on the prediction capability of Eq. (37). Material: CFRP

The very similar α values raises the question whether this parameter is actually material dependent, or rather it can be considered a constant of general applicability. At this aim, the minimum and maximum α values found ($\alpha = 1.30$ and 1.42) were alternatively fixed for all the materials and the related K values, best-fitting the experimental points were calculated and reported in Table 7.

The results are graphically shown in Fig. 52 for CFRP: the curves concerning a single material are very close with each other, so that the scatter in the experimental data does not allow to judge which of them is the most efficient in predicting penetration energy. The same was found for GFRP and PC. The assumption that

a single α value has a general applicability cannot be rejected. However, if this was the case, the application of Eq. (37) would be straightforward, and the parameter K alone could be used to rank different materials on the basis of their energy absorbing capacity.

3.7.2 Effect of Projectile Velocity

To ascertain the effect of loading speed on the penetration energy, static and dynamic impact tests were carried out on C50/50 and SMC (Table 1), with the same impactor and support diameter. A strong dependence of the energy absorbing capability of GFRP on the speed was found, approximately doubling when the loading speed increases from 2 mm/min to about 7 m/s. The discussed influence about flat GFRP panels has been observed by many researchers [58, 83, 84] whereas other data [53, 58] show that laminates made by graphite fibre are practically insensitive to loading speed. The sensitivity of GFRP to velocity reflects, so, the well known and discussed viscoelasticity of glass fibres and it is independent of the matrix behaviour. At this point, the same model about the prediction of the penetration energy was assessed also in the case of static tests demonstrating that the penetration energy is substantially unaffected by the loading speed. The latter and what previously said about indentation indicate that impact tests can be substituted by static tests if the response of a CFRP laminate in terms of indentation and penetration is under study.

From the results obtained, the authors [19] noted that small samples do not necessarily behave like an in-service component under impact conditions. Conversely, if the scope of a testing procedure is the material characterisation, the elastic energy absorbed by the specimens should be minimised. This suggests the use of clamps at the supports, and the lowest in-plane dimensions allowing a free development of the damage. Interestingly, from the results of a limited amount of tests carried out at high speed clamping the plates between circular rings 120 mm in diameter [19], the penetration energy was found coincident with what given by the beam tests, and at low velocity U_p was only slightly higher. Additional data about two different types of circular GFRP panels were discussed [77]: only a moderate increase in the penetration energy was found at the increase of the support diameter in the range 40 mm to 100 mm, although one of the laminates was quite thin (1.2 mm) and the plates were simply supported. From the previous results, it can be reasonably thought that, when specimen dimensions are up to about 120 mm, the elastic energy is low and test conditions adequate to yield a sufficiently accurate value of the material penetration energy are achieved.

Experimental evidence and theoretical justification of this behaviour was given in [19], where the authors performed penetration tests at both low and high velocity on CFRP using a simply supported beam configuration and varying the beam length. The penetration energy showed an increase well described by a simple analytical model that take into account the elastic deformation of the material. Additional data in this direction was discussed about GFRP panels [77]: a little increase in

the penetration energy of about 10% was found passing from 40 to 100 mm of the support diameter since the elastic energy to bend the panel up to the maximum load also increases, contributing to the overall energy stored by the structure. However, it is reasonable to think that up to about 120 mm of the specimen dimensions, the test conditions are adequate to yield accurate values of the penetration energy since in comparison the elastic energy is low and lower at increasing of the thickness.

3.7.3 Literature Survey

As a confirmation of the results found in this work, an extensive literature research is hereafter presented.

In [22, 23, 78], low-velocity impact tests were carried out on glass and carbon fibre reinforced plastics (GFRP and CFRP) having different thickness and volume fraction of reinforcement finding that the precision in the measured penetration energy was higher when U_p was plotted against the panel thickness, t, times fibre volume fraction, V_f, rather than against the actual thickness. The product $(t \cdot V_f)$ represents the total fibre thickness proportional to the total fibre areal weight. Therefore, the results obtained in literature seem to indicate that, for a given laminate, the total fibre content is the main parameter affecting penetration energy. It means that not only the resin content, but also its type negligibly affects the penetration energy. This was demonstrated in [22] where six types of resin, including a toughened epoxy, amorphous and semi-crystalline PEEK, and amorphous and semi-crystalline PPS, were used to fabricate quasi-isotropic GFRP laminates: little differences in impact behaviour were observed on the basis of matrix type.

Different forms of glass fibres (unidirectional, quadriaxial warp-knit fabric and eight-harness satin weave) were employed to obtain quasi-isotropic laminates with different spatial distribution of reinforcement [23]. The impact tests revealed that, for a given fibre areal weight, U_p was independent of the reinforcement architecture and stacking sequence and of the extend of the delamination, quite limited in some of the cases but considerable in some others. The latter could indicate that the energy associated with delamination phenomena is negligible compared to the overall penetration energy.

Additional data confirming the insensitivity of U_p to the fibre architecture can be found [77]: the energy absorbing capability of an in-plane isotropic sheet-moulding compound was shown to be practically coincident with that of the fabric laminates having the same fibre areal weight. Besides confirming the importance of the total fibre content, this result supports the hypothesis that the fibre orientations play a secondary role in determining the penetration response of a composite, at least when the anisotropy ratio is not too high. Also in what reported in [17, 21], the formula used for the calculation of the penetration energy involved the knowledge of the total fibre thickness, whereas the fibre orientations were not taken into account.

The penetration energy for a given laminate was first found to linearly increases with increasing t (i.e. fibre areal weight) [75, 76]. However, more recent data [17, 19, 21–23, 77, 78] demonstrate that U_p increases more than linearly with thickness. In particular, it was found that [17, 21], as already here demonstrated, the dependence of the penetration energy on the material thickness, t, for CFRP and GFRP laminates could be well described by a power law having exponent 1.5 and 1.35 respectively.

Also the impactor shape strongly influences U_p, which increases with increasing impactor dimensions. Most of the data available on this subject concern spherical indenters about 6–25.7 mm in diameter, although conically shaped and flat cylindrical tups have also been extensively used [4].

From the previous considerations, limiting the attention to spherical tups and a given fibre type, the most effective parameters in influencing U_p are the fibre areal weight and the impactor diameter, D_t. It is so necessary to establish a relationship correlating these quantities. It is very important to highlight the dependence of U_p on D_t. From Eqs. (36) and (37) confirmed by [17, 21], the effect of both the thickness and the impactor diameter could be modelled by power laws having practically the same exponent, it was suggested that the empirical relationship proposed here (Eq. 37) helps to predict the penetration energy. The experimental tests supported Eq. (37): all the data obtained substantially fall on a single master curve when plotted against the quantity ($t \cdot V_f \cdot D_t$) irrespective of the adopted tup diameter and fibre architecture and orientations. The formula proposed has a quite wide applicability with a typical value for α of about 1.4, and can be probably further simplified, allowing a simple comparison of different materials.

3.8 Residual Strength Model

Since the residual material properties after an impact are of primary concern in applying damage tolerance concepts, efforts were also made to correlate, analytically or experimentally, the residual strength and the impact energy and the damage mechanisms [9, 42, 85]. In literature some models have been proposed [9, 18–20] to predict the residual strength σ_c of a composite laminate after low velocity impact strength, as a function of the impact energy:

$$\frac{\sigma_c}{\sigma_o} = \sigma(U) \tag{40}$$

where σ_c and σ_o are the virgin and the material residual strength after impact, respectively.

Since an explicit form was found for the relationship between indentation depth and impact energy through the penetration energy (Eq. (32)), it is possible to predict the residual strength from indentation. If the compression strength is of concern, Eq. (40) can assume a complicated form, because of the effect of delamination on the failure modes precipitating final collapse.

Table 8 Experimental values of the constants $U_{\sigma o}$ and α in Eq. (41), and theoretical limit indentation, I_{lim}, beyond which a reduction in tensile strength is predicted

Laminate	$U_{\sigma o}$ (J)	α	I_{lim} (J)
$(\pm 30)_{2s}$	1.87	0.386	0.125
$(\pm 45)_{2s}$	1.97	0.267	0.143
$(\pm 60)_{2s}$	1.48	0.275	0.069

Even if models are available in the literature for the prediction of the residual strength, in this work, the formula proposed in [19] is assumed for the simplicity in the procedures required to evaluate the constants involved:

$$\frac{\sigma_c}{\sigma_o} = \left(\frac{U_{\sigma o}}{U}\right)^{\alpha} \tag{41}$$

σ_o is the virgin strength of the laminate, and $U_{\sigma o}$, α are two constants to be experimentally determined.

When $U = U_{\sigma o}$ the residual tensile strength equals the virgin material strength. $U_{\sigma o}$ physically represents the limit energy below which no strength reduction is found. Equation (41) predicts a monotonic decrease in the residual strength with increasing U. On the contrary, it is known that, beyond penetration, σ_c does not decrease further, remaining approximately constant or undergoing a small recovery. The previous considerations bring to the conclusion that Eq. (41) no longer holds for $U < U_{\sigma o}$ and $U > U_p$.

Noting that the reduction in tensile strength is dependent on the broken fibres, rather than on the delaminated area induced by impact, it was suggested [19] that $U_{\sigma o}$ could be directly measured as the area under the force-displacement curve up to the point of the first fibre breakage. This damage is often signalled by a sudden drop in the contact force (point b in Fig. 1).

Since the evidence of the first fibre failure in the force-displacement diagrams for all the laminates considered and labelled as T30, T60 and T45 in Table 1, the procedure proposed [19] for the calculation of the constants was followed also here. The $U_{\sigma o}$ values obtained for the materials tested are reported in Table 8.

The results that the $(\pm 30)_{2s}$ and $(\pm 60)_{2s}$ laminates exhibited a quite different $U_{\sigma o}$ was unexpected. They both should yield the same response to impact since the axial symmetry, being nominally identical.

The constant α appearing in Eq. (41) was evaluated for each laminate using the residual strength measured after a 7 J impact (last column in Table 8). At this energy value, no penetration was observed for the materials tested, so that the condition $U < U_p$, necessary to ensure the validity of Eq. (41), was fulfilled. Using the constants from Table 8 in Eq. (41), the continuous lines in Fig. 53 were drawn.

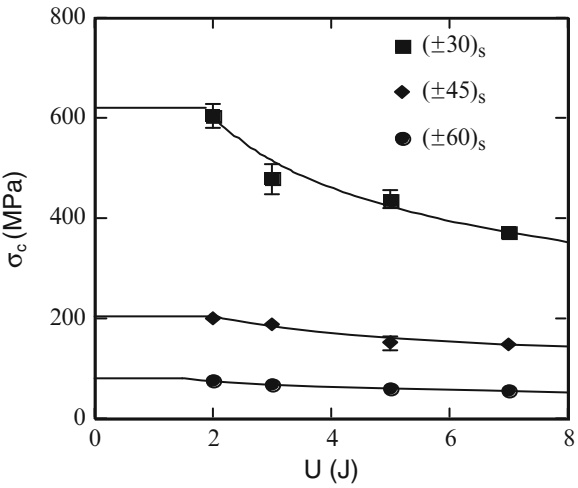

Fig. 53 Residual strength, σ_c, vs impact energy, U. *Black points*: test results. Solid lines: predictions on Eq. (41).

The correlation between the theoretical predictions and the experimental data (black symbols in Fig. 53) is very good, supporting the residual strength model.

Solving Eq. (39) for U, and substituting in Eq. (41), it results in:

$$\frac{\sigma_c}{\sigma_o} = \left[\frac{U_{\sigma o}}{U^*_{op} \cdot W^p} \left(\frac{I_o}{I} \right)^{1/\beta} \right]^{\alpha} \tag{42}$$

which yields the correlation wanted between I and σ.

For what previously shown in the indentation paragraph, the values $I_o = 6.77$ mm, $\beta = 2.535$, $U^*_{po} = 7.22$ J/(Kg/m^2)^p and $p = 1.50$, have a quite general applicability for laminates made of T400/934 layers, independently of the reinforcement architecture and fibre orientations. Taking this in mind, Eq. (42) becomes:

$$\frac{\sigma_C}{\sigma_O} = \left[\frac{U_{\sigma O}}{7.22 \cdot W^{1.50}} \left(\frac{6.77}{I} \right)^{\frac{1}{2.535}} \right]^{\alpha} \tag{43}$$

Contrary to the previous constants, here $U_{\sigma o}$ and α are characteristics of the specific laminate under concern, giving information on its resistance to first fibre breakage ($U_{\sigma o}$), and its sensitivity to impact damage in terms of residual strength (α).

Using Eq. (43) with the data in Table 8, the residual tensile strength for the three laminates tested having lay-ups $(\pm 30)_{2s}$, $(\pm 60)_{2s}$, and $(\pm 45)_{2s}$,was calculated as a function of the indentation I. The experimental data demonstrate a very reasonable agreement with theory, confirming the possibility to reliably predict the residual strength from the measured I value. In Fig. 54, it is shown for brevity only for the (±30) laminates but the same agreement with the same accuracy was found for the other orientations.

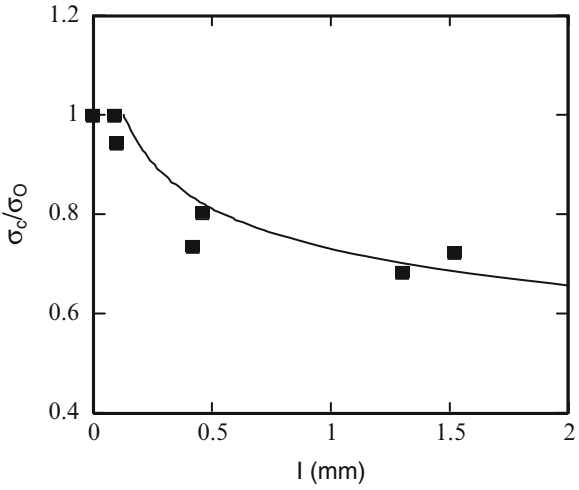

Fig. 54 Non-dimensional residual strength, σ_c/σ_o, against indentation, I, for $(\pm 30)_{2s}$ laminate

Solving Eq. (42) for $\sigma_c/\sigma_o = 1$, the limit value for I, I_{lim}, is obtained, under which no residual strength loss is expected:

$$I_{\text{lim}} = I_o \cdot \left(\frac{U_{\sigma o}}{U_{op}^* \cdot W^p} \right)^{\beta} \tag{44}$$

It is reported in the last column in Table 8 where it is observed that the initial strength decrease corresponds to an indentation level hardly detectable by visual inspection, especially for the $(\pm 60)_{2s}$ composite.

For a given laminate, Eq. (42) can be simplified in the form:

$$\frac{\sigma_c}{\sigma_o} = \left(\frac{I_o}{I_{\text{lim}}} \right)^{\gamma} \tag{45}$$

where:

$$\gamma = \frac{\alpha}{\beta} \tag{46}$$

Consequently, plotting on a log-log scale the residual strength data as a function of indentation for $I \geq I_{lim}$ results in a straight line providing a powerful tool for the calculation of the constants in Eq. (46), based on a minimum of experiments.

The analytical model evaluating the residual tensile strength as a function of indentation depth results in very reasonable agreement with the experimental data. In the particular case of a fixed laminate, the model becomes particularly simple, allowing the calculation of the material constants by a minimum of experimental tests.

It is important to note that, in some practice cases such as in aeronautics, impact damage strongly influences the design allowable in compression, rather than in tension. Therefore, the philosophy followed here could be usefully applied only if an analytical correlation similar to Eq. (41) should be found between the material compression strength and impact energy. Also the viscoelastic recovery of indentation during service, signalled by some researchers like in [86], deserves careful considerations and limits the applicability of the method to accidental damages produced during fabrication and control operations.

3.9 Energy Absorption Mechanisms and Damage: Correlation

The scope of this section is to establish a correlation between the damage occurring in a composite as a consequence of low-velocity impact and the energy dissipated during the impact phenomenon. Instrumented impact tests at different energy levels were at this aim carried out on glass fabric/epoxy laminates having different thicknesses (G in Table 1). To assess damage progression as a function of impact energy, ply-by-ply delamination and fibre breakages were measured by destructive tests deplying the specimens with the help of a heat source. A previous model [29], based on energy balance considerations, was applied for the interpretation of the experimental results. Some limitations in its applicability, supporting the present work, are emphasized. The contribution of fibre breakage and matrix damage to the irreversibly absorbed energy was found to be comparable at low impact energies; with increasing initial energy levels, delamination becomes predominant in determining energy dissipation.

3.9.1 Energy Absorbed by Fiber and Matrix Failures

It is important to understand the mechanisms of energy absorption in a laminate during low-velocity impact. Delfosse and Poursartip [29] tried to identify those mechanisms and correlated energy losses with observed failure modes. They carried out impact tests at different energy levels on two CFRP laminates, the first one (based on an IM6/937 material system) characterized by a brittle matrix, and the other (T800H/3900-2) by a ductile one. Following the authors, the absorbed energy, U_a, has two components, one, U_{dam}, necessary to create the damage, and the other, U_{dis}, dissipated through vibrations, heat, inelastic behaviour of the projectile or the supports, and so forth.

Since three types of damage are possible to occur in a laminate subjected to impact, and so the associated energies namely permanent indentation, U_{pi}, matrix damage (delamination and intraply splitting), U_m, and fibre breakage, U_f

$$U_a = U_{pi} + U_m + U_f + U_{dis} \tag{47}$$

On the other hand, it can be put:

$$U_m = G_m \cdot A_m \tag{48}$$

$$U_f = G_f \cdot A_f \tag{49}$$

where A_m is the total area of matrix damage, A_f the total area of broken fibres and G_m, G_f, are the energies required to create a unit damage area in the matrix and fibre, respectively.

The total delaminated area, A_m, was evaluated by pulse-echo ultrasonics together with destructive inspection whereas A_f, was measured thermally deplying the impacted panels after the resin was burnt off in a furnace.

Three-point bending tests were carried out to estimate G_f whereas the measurement of G_m was quite laborious, involving the selection of a range of impact energies giving rise uniquely to delamination damage, without fibre breakage: G_m was given by the slope of the straight line correlating U_a and A_m. However, this range of energies related only with delamination was very small (about 4.5 J) in the tough laminate, resulting in not accurated determination of G_m for the T800H/3900-2 system.

After the comparison between the absorbed energy deriving from matrix and fibre failure and the total absorbed energy [29], it was concluded that the contribution of the quantity ($U_{pi} + U_{dis}$) to U_a is negligible. In this case:

$$U_a \approx G_m A_m + G_f A_f \tag{50}$$

Delfosse and Poursartip found $G_m = 0.8$ KJ/m^2 and $G_m = 5.0$ KJ/m^2 for the brittle and the tough system, respectively. The fracture toughness value, G_{IIc} were obtained from quasi-static fracture toughness experiments, 0.75 KJ/m^2 and 2.0 KJ/m^2 and the big difference between G_m and G_{IIC} for the tough resin suggested that other damage mechanisms, not caught by the measured delaminated area, could contribute significantly to energy absorption mechanism.

Here, the main scope is to assess a method of data reduction able to overcome the difficulties previously highlighted.

After impact on the G laminates (Table 1), the projected delaminated area was obtained exploiting the translucent appearance of the material: the damage zone was highlighted by an intense light source on the back of the specimens; then, the photographed damaged area was measured by an image analyzer.

Moreover, in order to study the ply-by-ply damage extent and type, a central hole 1 mm in diameter was drilled in correspondence of the impact point of selected specimens. The latter were, then, immersed in black ink. Through the hole the liquid easily penetrated into the interlaminar cracks until the projected delaminated area was completely darkened by the ink; then, they were dried and carefully deplied with the help of moderate heating. The delaminated area in correspondence of each

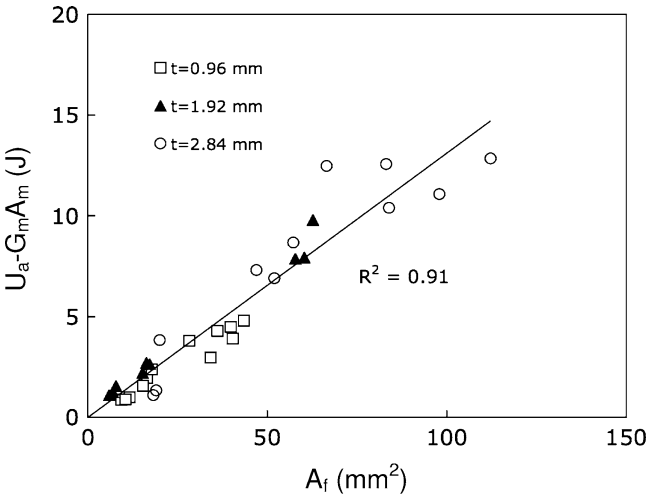

Fig. 55 Calculation of the upper bound value of unit energy for fibre breakage

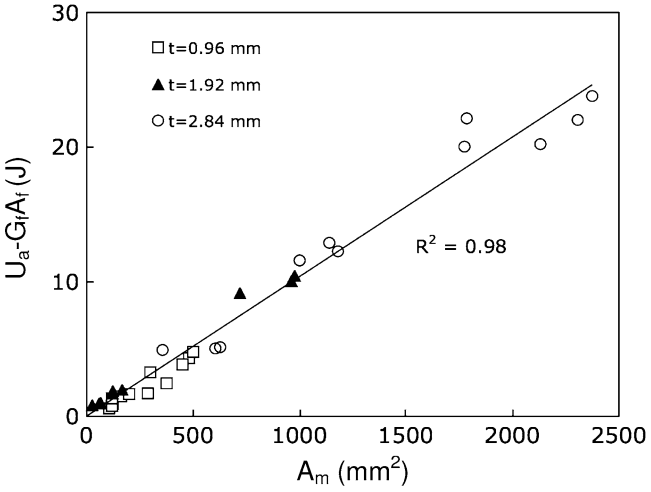

Fig. 56 Calculation of the upper bound value of unit energy for matrix damage

interlaminar surface was measured and the in-plane length of broken fibres within each ply was evaluated by optical microscopy at low magnification, following the procedure adopted by Delfosse and Poursartip [29].

If $(U_{pi} + U_{dis})$ in Eq. (47) is disregarded, it is possible to calculate G_f^u and G_m^l from the slope of the straight line passing through the origin in Figs. 55 and 56 where U_a-G_mA_m and U_a-G_fA_f obtained from Eqs. (47), (48), and (49), are reported against A_f and A_m respectively. The index "u" ("l") stand for an upper (lower) bound value. At the same way the $G_m{}^u$ and $G_f{}^l$ values can be obtained plotting A_m against

Table 9 Upper and lower unit energies bound values for matrix damage and fibre breakage

G_f^u (KJ/m^2)	G_f^l (KJ/m^2)	G_m^u (KJ/m^2)	G_{mf}^l (KJ/m^2)
131.0	126.3	10.1	10.4

U_a-G_fA_f. Tentative values was assumed for this quantity changing it until the best-fit straight line fitting the experimental data follows the expected trend. A lower limit of the absorbed energy, U_{amin}, was calculated considering the lower values of G_f and G_m.

The best-fit straight lines shown in the figures were drawn through all the data points. The straight lines fit reasonably well the experimental trends, supporting the applicability of the energy criterion proposed in [29].

In Table 9, the G_f^u, G_f^l,G_m^l, G_m^u values obtained from Figs. 55 and 56, are collected. It is possible to note that, in agreement with what find by Delfosse and Poursartip [29], the unit energy associated with fibre breakage is far higher than its matrix counterpart but the latter is about five times higher than what usually measured in a Mode II delamination test for a tough resin [87].

3.9.2 Delaminated Area and Broken Fiber Length

After impacting the G panels with two different impactor diameters, 19.8 and 16 mm, the extent of the projected delaminated area was obtained exploiting the translucent appearance of the material: the damaged zone was highlighted by an intense light source on the back of the specimens, photographed and the area was measured by an image analyzer. Two parameters, i.e. the projected delaminated area, A_p, the area of delamination as perceived from visual observation and the visible broken fibre length, d, were here assumed. The visible broken fibre length were obtained by measuring the length of the two lines along which fibre fracture was observed. Their mean value was, then, calculated. It is important to underline that A_p and d must not be confused with the corresponding ply-by-ply damage, with which the absorbed energy is conceivably correlated.

In Fig. 57, a typical impact damage visually observed on to the back face of the panel, where the classical visible diamond-shaped delaminated area attained its maximum dimensions, is shown. The axes coinciding with the warp-weft directions of the surface fabric layer (horizontal and vertical directions), is clearly visible. Besides, fibre fractures occur along two lines of length slightly lower than the major axes of delamination.

From Fig. 57, other cross fibre failures in the internal layers oriented at 45°, were also observed together with multiple delaminations occurring along the thickness suggested by a darker area fully contained in the projected delamination. These damages are not taken into account for A_p and d.

The behaviour of d and A_p with impact energy is shown in Figs. 58 and 59, respectively. Each point is related to a single measurement and the different symbols

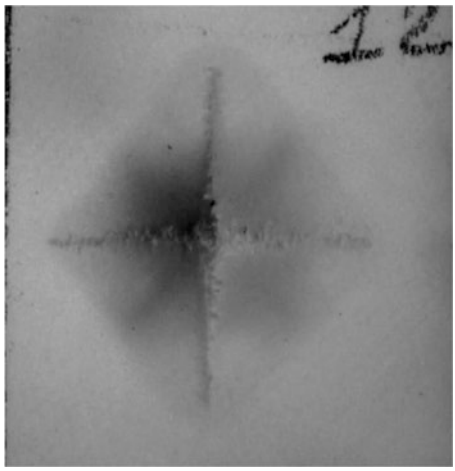

Fig. 57 Typical damage zone after impact. *Back surface*. Panel thickness t = 1.92 mm. Tup diameter D_t = 16 mm. Impact energy U = 15.8 J

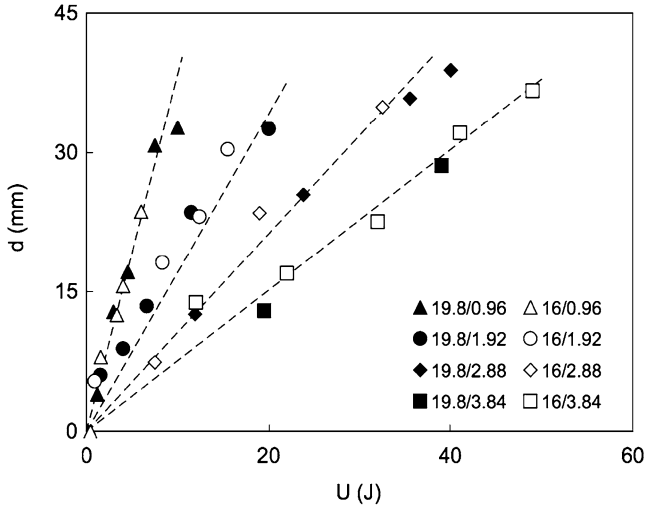

Fig. 58 Effect of the panel thickness, *t*, on the evolution of visible broken fibre length, *d*, at the increasing of impact energy, *U*. *Dashed lines*: Eq. (51)

are identified by the label "A/B", where A is the impactor diameter and B the panel thickness in mm.

It is clear that d and A_p are unaffected by the tup diameter and an increase was noted with decreasing the panel thickness, for a fixed value of the impact energy U. The visible broken fibre length vary linearly with U following the empirical equation (dashed lines in Fig. 58):

$$d = k\frac{U}{t^{\alpha}} \tag{51}$$

with $\alpha = 1.17$, $k = 3.66$ mm$^{(1+\alpha)}$/J.

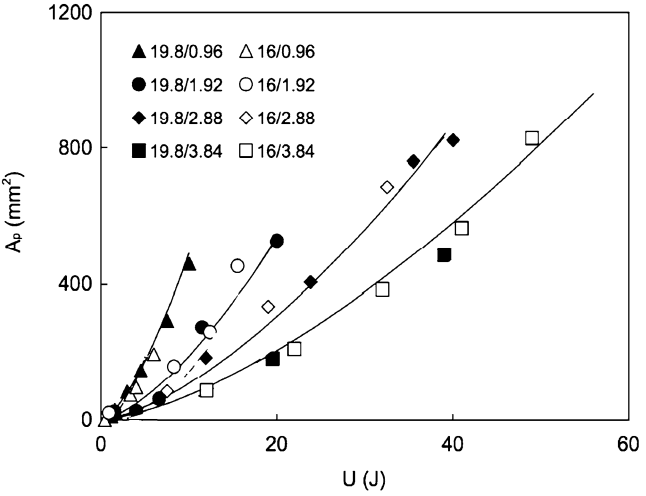

Fig. 59 Projected delaminated area, A_p, versus impact energy, U. *Solid lines*: Eq. (52)

The dependence of A_p on impact energy is represented by the relationship (solid lines in Fig. 59):

$$A_p = 14.71 \frac{U^{1.50}}{t^{1.38}} \tag{52}$$

providing A_p (in mm^2), if U (in J) and t (in mm) are known.

Equations (51) and (52) describe the role played by impact energy and laminate thickness in determining visual damage.

The study about the mechanisms of damage initiation and propagation was the primary focus of this part of the research. At the aim to find a simple impact parameter for the prediction of the delaminated area, the main factors causing delamination were here studied so that the possibility to correlate internal and external damage. As already said, there has been a considerable debate about the relative merits of using force and energy as a scale parameter for this impact damage. The approach based on impact force works well in different applications, especially when the onset of damage has to be determined for different plate or impactor geometry [47, 48] whereas Delfosse and Poursatip [29] showed that an energy-based approach can be more helpful in examining the extent of damage, beyond the onset.

On the base of what above asserted about the independence of the loading velocity [53–55], static tests were here carried out on rectangular carbon fibre reinforced plastic plates of four different thickness (T in Table 1). In order to verify the effect of the impactor, a number of impact tests were carried out varying the indentor diameter too. After the experimental tests, the specimens were subjected to non-destructive evaluation using an ultrasonic C-scan apparatus to investigate about the delamination extent. Moreover, some specimens were sectioned and observed by optical microscopy to confirm the US results.

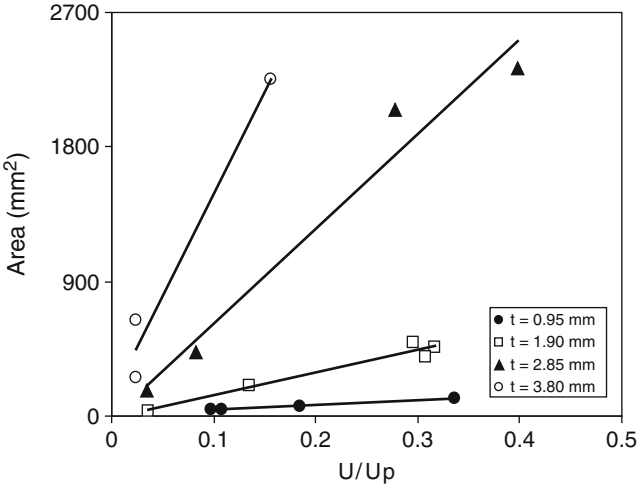

Fig. 60 Delaminated area versus non-dimensional energy, U/U_p, for laminates different in thickness, t

The most common parameter [25, 29, 42, 79, 88, 89], the impact energy considered the right one to evaluate the delaminated area is first investigated. However, the force approach was revealed in this case more interesting in collecting all the experimental data on a single master curve.

Discussion

The data presented refer to different material system, different thickness, different architecture, (unidirectional, fabric, cross ply, etc.) [79, 90, 91].

It could be interesting to find a way, as already done for the indentation, to obtain a single master curve for experimental data, about a specific material system, obtained in different test conditions, like different impactor, different thickness, different support diameter etc. A single master curve could also allow to know the threshold energy, given by the x intercept, below which no damage is present in the material.

With this in mind, the extension of the delaminated area against the non-dimensional energy U/U_p measured on the T laminates (Table 1), is shown in Fig. 60. The different symbols refer to the different thickness and the straight lines are drown to better understand the experimental data trend. First of all, it is important to note that the maximum energy level for each thickness is less than 40% of the penetration energy. This is due to the fact that the low energy range is the most interesting in aeronautical field because of the presence of a consistent internal damage correspondent to a not so evident external indentation. Moreover,

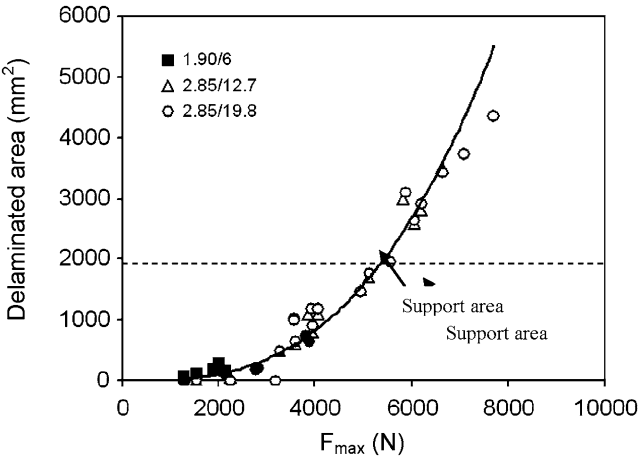

Fig. 61 Delaminated area versus impact load for laminates different in thickness

contrarily to what happens for the indentation, the experimental points are separated again. This means that the impact energy is not a simple parameter to adopt for the prediction of the delaminated area.

The fact already noted that the same energy level produces a larger delaminated area in thickest panels could be explained with the fact that the thickness laminates absorb the same energy with an higher load since the material rigidity increases with the thickness raised to the 3rd power. The latter suggests that the delaminated area can be related to the impactor-material contact load that could be used as a parameter to compare and to predict impact damages in structures from coupon tests [34]. Even if there is an open debate, the approach based on impact force works well in many applications, especially when the onset of damage has to be determined for different plates or impactor geometries [34, 49–51, 72, 73].

So said, the same experimental point from Fig. 60 are plotted in Fig. 61 against the maximum contact load, F_{max}: a single master curve was found and the damage is again larger the thicker the laminates are.

Support area

The continuous curve is the graphical representation of the following equation:

$$A = \eta \cdot F_{max}^{\beta} \tag{53}$$

where A is the delaminated area. The value of the two constants obtained by the minimum square method is $\eta = 3.13 \times 10^{-8}$ mm^2/N$^{\beta}$ and $\beta = 2.89$.

On the base of what found, the impact force could be used as a parameter to compare and to predict impact damage in structures from coupon tests [47].

4 Conclusion

Static and low velocity impact tests were carried out on different composite laminates in different tests conditions, at the main scope to supply more information about their behaviour under dynamic load conditions. The authors faced the very complex problem of the failure modes caused by an impact and tried to correlate them to the main parameters involved in the phenomenon at the aim to obtain semi empirical and analytical models for the prediction of the residual strength.

The main conclusions are listed in the following.

- The force required for damage initiation under form of delamination increases following a power law whose exponent is very close to 1.5 observed for the contact law. From the observation of the failure modes, this suggests that delamination is mainly due to shear stresses, which can be calculated by the contact law.
- The analysis highlighted the importance of the penetration energy in giving the possibility to predict the impact energy by a simple indentation measurement. The scope was the assessment of a simple model to correlate the indentation depth and the energies involved in the impact phenomenon. The model was found to have a quite general applicability: for a given fibre/resin system, the indentation depth is substantially independent of fibre type, architecture and orientations, laminate thickness and resin type and content, varying only as a function of the impact energy to the penetration energy ratio.
- The penetration energy can be predicted by an empirical equation: a power law with the exponent that is a constant, scarcely influenced by matrix type and content; the reinforcement architecture and orientations, and support diameter, play a minor role too in affecting U_p. The main parameter determining the energy absorption capacity is the total fibre thickness, proportional to the total areal weight of reinforcement and given by the product $(t \cdot V_f)$ of the panel thickness times the fibre volume fraction (Eq. (37)). This parameter was revealed useful in normalising impact data obtained under different test conditions.
- An analytical model evaluating the residual tensile strength as a function of indentation depth results in very reasonable agreement with the experimental data. The model allows the calculation of the material constants by a minimum of experimental tests.
- An elastic solution available for circular isotropic plates loaded at the centre was modified to model the indentation and applied to the prediction of the load-displacement curve. The analytical model accurately describes the elastic behaviour of the plates allowing to know the first failure energy. The prediction of the energy reveals that for thin plates, a large portion of the stored energy is correlated with the non-linear response of the plate deriving from the achievement of the large displacements regime and the indentation was negligible. The cubic component in Eq. (22) plays a major role in determining the plate response. This energy becomes negligible for thick plates (the influence of the

cubic component in Eq. (22) becomes lower and lower); the energy due to the local contact phenomena must be taken into account.
- The caused damages were observed by visual analysis, as well as by deplying some of the specimens: contrarily to what usually found, delamination was found between layers equally oriented too.

References

1. Sun CT, Liou WJ (1989) Investigation of laminated composite plates under impact dynamic loading using a three-dimensional hybrid stress finite element method. Comput Struct 33(3):879–884
2. Cairns DS (1991) Simple elasto-plastic contact laws for composites. J Reinf Plast Compos 10(4):423–433
3. Bucinell RB, Nuismer RJ, Koury JL (1991) Response of composite plates to quasi-static impact events. In: O'Brien TK (ed) Composite materials: fatigue and fracture. ASTM STP 1110., pp 528–549
4. Abrate S (1994) Impact on laminated composites: recent advances. Appl Mech Rev 47(11):517–544
5. Hong S, Liu D (1989) On the relationship between impact energy and delamination area. Exp Mech 29(2):115–120
6. Hull D, Shi YB (1993) Damage mechanism characterisation in composite damage tolerance investigations. Compos Struct 23:99–120
7. Hitchen SA, Kemp RMJ (1995) The effect of stacking sequence on impact damage in a carbon fibre/epoxy composite. Composites 26:207–214
8. Richardson MOW, Wisheart MJ (1996) Review of low-velocity impact properties of composite materials. Composites A 27A:1123–1131
9. Caprino G (1984) Residual strength prediction of impacted CFRP laminates. J Compos Mater 18:508–518
10. Cantwell WJ, Morton J (1991) The impact resistance of composite materials – a review. Composites 22(5):347–362
11. Cairns DS, Minuet PJ, Abdallah MG (1993) Theoretical and experimental response of composite laminates with delaminations loaded in compression. Compos Struct 25:113–120
12. Kim J-K, Mackay DB, Mai Y-W (1993) Drop-weight impact damage tolerance of CFRP with rubber-modified epoxy matrix. Composites 24(6):485–494
13. Choi HY, Downs RJ, Chang F-K (1991) A new approach toward understanding damage mechanisms and mechanics of laminated composites due to low velocity impact: part I-experiments. J Comp Mater 25:992–1011
14. Choi HY, Chang FK (1992) A model for predicting damage in graphite/epoxy laminated composites resulting from low-velocity point impact. J Compos Mater 26(14):2134–2169
15. Abrate S (1998) Impact on composite structures. Cambridge University Press, Cambridge
16. Timoshenko SP, Woinowsky-Krieger S (1959) Theory of plates and shells. McGraw-Hill, Singapore
17. Caprino G, Lopresto V (2000) The significance of indentation in the inspection of CFRP panels damaged by low-velocity impact. Compos Sci Technol 60:1003–1012
18. Chang FK, Choi HY, Wang HS (1990) Damage of laminated composites due to low velocity impact. In: 31st AIAA/ASME/ASCE/AHS/ASC structures, structural dynamics and Materials conference, Long Beach, CA, 2–4 April 1990, pp 930–940
19. Cantwell WJ, Morton J (1990) Impact perforation of carbon fibre reinforced plastics. Compos Sci Technol 38:119–141

20. Husman GE, Whitney JM, Halpin JC (1975) Residual strength characterisation of laminated composites subjected to impact loading. ASTM STP 568:92–113
21. Delfosse D, Poursartip A (1985) Experimental parameter study of static and dynamic out-of-plane loading of CFRP laminates. In: Proceedings of the 10th international conference on composite materials (ICCM10), Whistler, Canada, August 1985, pp V-583-590
22. Bibo G, Leicy D, Hogg PJ, Kemp M (1994) High-temperature damage tolerance of carbon fibre-reinforced plastics. Part 1: impact characteristics. Composites 25(6):414–424
23. Bibo GA, Hogg PJ (1998) Influence of reinforcement architecture on damage mechanisms and residual strength of glass-fibre/epoxy composite systems. Compos Sci Technol 58:803–813
24. Caprino G, Lopresto V, Scarponi C, Briotti G (1999) Influence of material thickness on the response of carbon-fabric/epoxy panels to low-velocity impact. Compos Sci Technol 59:2279–2286
25. Ghasemi Nejhad MN, Parvizi-Majidi A (1990) Impact behaviour and damage tolerance of woven carbon fibre-reinforced thermoplastic composites. Composites 21(2):155–168
26. Caprino G, Langella A, Lopresto V (2002) Elastic behaviour of circular composite plates transversely loaded at the centre. Composites A 33:1191–1197
27. Schoeppner GA, Abrate S (2000) Delamination threshold loads for low velocity impact on composite laminates. Composites A 31:903–915
28. Sjoblom PO, Hartness TM, Cordell TM (1988) On low-velocity impact testing of composite materials. J Compos Mater 22(1):30–52
29. Delfosse D, Poursatip A (1997) Energy-based approach to impact damage in CFRP laminates. Composites A 28A:647–655
30. Liu S, Kutlu Z, Chang FK (1993) Matrix cracking and delamination propagation in laminated composites subjected to transversely concentrated loading. J Compos Mater 27(5):436–470
31. Herup EJ, Palazotto AN (1997) Low-velocity impact damage initiation in graphite/epoxy/Nomex honeycomb-sandwiche plates. Compos Sci Technol 57(12):282–289
32. Yang SH, Sun CT (1982) Indentation law for composite laminates. In: Daniel I (ed) Composite materials: testing and design (sixth conference), ASTM STP 787, pp 425–449
33. Tan TM, Sun CT (1985) Use of statical indentation laws in the impact analysis of laminated composite plates. J Appl Mech 52(8):6–12
34. Jackson WC, Poe CC Jr (1993) The use of impact force as a scale parameter for the impact response of composite laminates. J Compos Technol Res 15(4):282–289
35. Abrate S (2001) Modeling of impacts on composite structures. Compos Struct 51:129–138
36. Timoshenko SP Strength of materials. McGraw-Hill, New York
37. Chang FK, Choi HY, Wang HS (1990) Damage of laminated composites due to low velocity impact. In: 31st AIAA/ASME/ASCE/AHS/ASC structures, structural dynamics and materials conference, Long Beach, CA, 2–4 April 1990, pp 930–940
38. Stout MG, Koss DA, Liu C, Idasetima J (1999) Damage development in carbon/epoxy laminates under quasi-static and dynamic loading. Compos Sci Technol 59:2339–2350
39. Gosse JH, Mori PBY (1988) Impact damage characterization of graphite/epoxy laminates. In: Proceedings of the 3rd technical conference of the American Society for Composites, Seattle, WA, pp 334–353
40. Tsai SW, Hahn HT (1975) Introduction to composite materials. Technomic Publishing Company, Lancaster
41. Hashin Z (1975) Failure criteria of unidirectional fiber composites. J Appl Mech 47:329–334
42. Liu S (1994) Quasi impact damage initiation and growth of thick-section and toughened composite materials. Int J Solids Struct 31(22):3079–3098
43. Siow YP, Shim PW (1998) An experimental study of low velocity impact damage in woven fiber composites. J Compos Mater 32(12):1178–1202
44. Kaczmerek H (1995) Ultrasonic detection of damage in CFRPs. J Compos Mater 29:59–95
45. Hosur MV, Murthy CRL, Ramamurthy TS, Shet A (1998) Estimation of impact-induced damage in CFRP laminates through ultrasonic imaging. NDT&E Int 31:359–374

46. Olsson R (2001) Analytical prediction of large mass impact damage in composite laminates. Composites A 32:1207–1215
47. Sjoblom P (1987) Simple design approach against low velocity impact damage. In: Proceedings of 32nd SAMPE symposium, Anaheim, CA, pp 529–539
48. Caprino G, Langella A, Lopresto V (2003) Prediction of the first failure energy of circular carbon fibre reinforced plastic plates loaded at the centre. Composites A 34:349–357
49. Zhang X (1998) Impact damage in composite aircraft structures-experimental testing and numerical simulation. Proc Inst Mech Eng 212(4):245–259
50. Davies GAO, Zhang X, Zhou G, Watson S (1994) Numerical modelling of impact damage. Composites 25(5):342–350
51. Davies GAO, Zhang X (1995) Impact damage prediction in carbon composite structures. Int J Impact Eng 16(1):149–170
52. Olsson R (1999) A review of impact experiments at FFA during 1986 to 1998. The Aeronautical Research Institute of Sweden, FFA TN 1999–08
53. Lesser AJ, Filippov AG (1991) Kinetics of damage mechanisms in laminated composites. In: International SAMPE symposium and exhibition, vol 36, part 1, pp 886–900
54. Crivelli Visconti I, Caprino G, Di Ilio A, Carrino L (1983) Impact tests on CFRP: a static-dynamic analogy. In: High performance composite materials – new applications and industrial production, acts of 4th international SAMPE conference-SAMPE Euro chapter, Bordeaux, 17–20 October 1983, pp 189–196
55. Lesser AJ, Filippov AG (1991) Kinetics of damage mechanisms in laminated composites. In: International SAMPE symposium and exhibition, vol 36, part 1, pp 886–900
56. Srinivasan K, Jackson WC, Hinkley JA (1991) Response of composite materials to low velocity impact. In: International SAMPE symposium and exhibition, vol 36, part 2, pp 850–862
57. Shivakumar KN, Elber W, Illg W (1985) Prediction of low velocity impact damage in thin circular laminates. AIAA J 23(3):442–449
58. Caprino G, Crivelli Visconti I, Di Ilio A (1984) Composite materials response under low-velocity impact. Compos Struct 2:261–271
59. Wu E, TSai CZ, Chen YC (1994) Penetration into glass/epoxy composite laminates. J Compos Mater 28:1783–1802
60. Zenkour AM, Mashat DS (2009) Exact solutions for variable-thickness inhomogeneous elastic plates under various boundary conditions. Meccanica 44(4):433–447
61. Agarwal BD, Broutman LJ (1980) Analysis and performance of fiber composites. Wiley, New York
62. Grediac M (1999) A procedure for designing laminated plates with required stiffness properties. Application to thin quasi-isotropic quasi-homogeneous uncoupled laminates. J Compos Mater 33:1939
63. Park JW, Kim YH (1999) Predictor-corrector procedure for displacements, stresses and their sensitivity coefficients in composite panels. J Compos Mater 33:1222
64. Wang CM, Reddy JN, Lee KH (2000) Shear deformable beams and plates. Elsevier, Amsterdam
65. Scarponi C, Briotti G, Barboni R, Marcone A, Iannone M (1996) Impact testing on composite laminates and sandwich panels. J Compos Mater 30(17):1873–1911
66. Lagace PA, Wolf E (1993). Impact damage resistance of several laminated material systems. In: 34th AIAA structures, structural dynamics and materials conference, La Jolla, CA, Pt. 4, pp 1863–1872
67. Lopresto V, Caprino G (2002) Elastic response of circular CFRP plates under low-velocity impact. In: Proceedings of ECCM10, 3–7 giugno 2002, Bruge, Belgio
68. Sun CT, Chen JK (1985) On the impact of initially stressed composite laminates. J Compos Mater 19:490–503
69. Davies GAO, Hitchings D, Wang J (2000) Prediction of threshold impact energy for onset of delamination in quasi-isotropic carbon/epoxy composite laminates under low-velocity impact. Compos Sci Technol 60:1–7

70. Cartiè DDR, Irving PE (2002) Effect of resin and fibre properties on impact and compression after impact performance of CFRP. Composites A 33:483–493
71. Lopresto V, Melito V, Leone C, Caprino G (2006) Effect of stitches on the impact behaviour of graphite/epoxy composites. Compos Sci Technol 66/2:233–239
72. Lagace PA, Williamson JE, Tsang PHW, Wolf E, Thomas SA (1993) A preliminary proposition for a test method to measure (impact) damage resistance. J Reinf Plast Compos 12(5):584–601
73. Poe Jr CC (1991) Relevance of impacter shape to non visible damage and residual tensile strength of a thick graphite/epoxy laminate. In: O'Brien TK (ed) Composite materials: fatigue and fracture, vol 3, ASTM STP 1110. American Society for Testing and Materials, Philadelphia, PA, pp 501–527
74. Sutherland LS, Guedes Soares C (2005) Impact on low fibre-volume, glass/polyester rectangular plates. Compos Struct 68:13–22
75. Wardle MW, Tokarsky EW (1983) Drop weight impact testing of laminates reinforced with Kevlar aramid fibres, E-glass and graphite. Compos Technol Rev 5(1):4–10
76. Hsieh CY, Mount A, Jang BZ, Zee RH (1990) Response of polymer composites to high and low velocity impact. In: Proceedings of the 22nd international SAMPE technical conference, 6–8 November 1990, pp 14–27
77. Caprino G, Lopresto V (2000) Factors affecting the penetration energy of glass fibre reinforced plastics subjected to a concentrated transverse load. In: ECCM–9, Brighton, 4–7 June 2000
78. Babic L, Dunn C, Hogg PJ (1989) Damage development and its significance in GRP subjected to impact. Plast Rubb Process Appl 12(4):199–207
79. Cantwell WJ, Morton J (1989) The influence of varying projectile mass on the impact response of CFRP. Compos Struct 13:101–104
80. Caprino G (1989) Results of instrumented drop-weight impact tests on polycarbonate and glass fibre reinforced plastics panels. Istituto Donegani internal report
81. Strait LH, Karasek ML, Amateau MF (1992) Effects of stacking sequence on the impact resistance of fiber reinforced thermoplastic toughened epoxy laminates. J Compos Mater 26(12):1725–1740
82. Chotard TJ, Benzeggagh ML (1998) On the mechanical behaviour of pultruded sections submitted to low-velocity impact. Compos Sci Technol 58(6):839–854
83. Wu E, Shyu K (1993) Response of composite laminates to contact loads and relationship to low-velocity impact. J Compos Mater 27(15):1443–1464
84. Wang H, Vu-Khanh T (1994) J Compos Mater 28:684
85. Cantwell WJ, Morton J (1990) An assessment of the residual strength of an impact-damaged carbon fibre reinforced epoxy. Compos Struct 14:303–317
86. Ilcewicz I (1997). Impact damage in composite structures. Polymer matrix composites, MIL-handbook 17
87. Davidson BD, Kumar M, Soffa MA (2009) Influence of mode ratio and hygrothermal condition on the delamination toughness of a thermoplastic particulate interlayered carbon/epoxy composite. Composites A 40:67–79
88. Scarponi C, Briotti G, Barboni R (1999) Reduction of tensile strength in angle-ply composite laminates due to low-velocity impact. J Reinf Plast Compos 18(1):63–85
89. Morton J, Godwin EW (1989) Impact response of tough carbon fibre composites. Compos Struct 13:1–19
90. Liu D (1988) Impact-induced delamination – a view of bending stiffness mismatching. J Compos Mater 22:674–692
91. Kumar P, Rai B (1993) Delaminations of barely visible impact damage in CFRP laminates. Compos Struct 23:313–318